4-23-2008

The Vibrational Behavior of a Cured Carbon Fiber Disk and a Tennis Racket

Nick Timme '08
Illinois Wesleyan University

The Vibrational Behavior of a Cured Carbon Fiber Disk and a Tennis Racket

Nick Timme

Advisor: Andrew Morrison

April 23rd, 2008

Abstract

In this project the vibrational behavior of a circular cured carbon fiber plate and a tennis racket is examined using a speckle-pattern interferometry system built and designed by students at Illinois Wesleyan University. Specifically, the mode shapes and mode frequencies are presented and discussed. With regards to the carbon fiber plate, the effects of the orthogonal construction of the plate on the vibrational behavior are studied. With regards to the tennis racket, the mode shapes of the racket are imaged for the first time using speckle-pattern interferometry. Furthermore, the effects of commercially available vibration dampers on the vibrational behavior of a tennis racket is also presented. In addition, the challenges of imaging various objects using speckle-pattern interferometry are explained, along with several methods for overcoming these challenges.

1: Introduction

Any object that vibrates possesses modes of vibration. These modes are manifest by very large amplitude vibrations when the object is driven at the mode frequency or resonance.[1] Any possible vibration the object can perform can be created by a linear combination of the mode shapes. The experimental goal of this project was to find and study the mode frequencies and mode shapes of a circular cured carbon fiber plate supported at its center and a tennis racket.

This study was conducted primarily using a speckle-pattern interferometry (SPI) system built and developed by students and faculty at Illinois Wesleyan University. This system allows for low cost, high quality, real time imaging of the vibrational behavior of various objects. Observing the vibrational behavior of an object is a non-destructive way to investigate the material properties of that object, as well as potentially search for damage and defects. For these reasons SPI systems can and have been employed in industry and research.

The two systems being studied, a carbon fiber disk and a tennis racket, were chosen for disparate reasons. Carbon fiber is widely used in industries of all types including aeronautics, the automobile industry, and the athletic industry. Due to its wide use, the vibrational behavior of carbon fiber is of interest to a large community. Many applications utilizing carbon fiber are subject to vibrations. For instance, the vibrations generated by an aircraft engine affect carbon fiber components in the aircraft. As a first step towards investigating those complex situations, it was decided that a relatively simple system should be the focus of this project. Thus, for the purposes of this project the simple carbon fiber system studied was a circular plate supported at its center.

[1] Throughout this paper the terms "mode frequency" and "resonance" shall be used interchangeably.

The behavior of an isotropic plate supported at its center has been well studied and some work has been done on the type of system studied here (an orthotropic plate supported at its center) [1 – 4]. However, this work has centered mainly on the mode frequencies of orthotropic plates and not on the mode shapes. In this project, both the mode frequencies and the mode shapes are studied, and special emphasis is placed on utilizing the SPI system to observe any effects the orthogonal nature of carbon fiber might have on the mode shapes.

The tennis racket was initially chosen as an object to study due to the challenge of simply imaging the vibrating racket head with the SPI system. We believed that the small surface area of the strings in the racket head would prevent production of satisfactory data. In attempting to image the tennis racket, though, it was found that the SPI system was capable of producing extremely high quality images of the vibrating racket. In fact, no research, as far as we are aware, has ever been conducted on the vibrational behavior of a tennis racket using SPI.

Tennis racket manufacturers are concerned about the vibrational characteristics of tennis rackets because the vibrational behavior of a racket influences its physical capabilities and the feeling experienced by the player when using it. Thus, using a system that has never been employed to study the vibrational behavior of tennis rackets may hopefully produce new insights.

One topic that has been studied regarding the vibrational behavior of tennis rackets is the effects, if any, of commercial vibration dampers have on the vibrational behavior of a tennis racket [5 – 8]. These dampers are advertised as reducing uncomfortable vibrations in the racket that lead to a bad "feel" on the part of the player. How the player experiences the racket is not the focus of this project. Rather, the effects of four commercially available vibration dampers on the vibrational behavior of the racket were studied. The SPI system was used to observe changes

in mode frequency, mode shape, and vibrational intensity caused by these vibration dampers. In order to evaluate the effects of the vibration dampers the racket was imaged with and without the vibration dampers in place. In doing so, not only was information gleaned regarding the effects of vibration dampers, but the vibrational behavior of an unaltered racket was also observed using the SPI system.

The layout of this paper is straightforward. First, the speckle-pattern interferometry system used for this project is described in conjunction with the theoretical basis for this system. Second, a brief background of cured carbon fiber plate and orthotropic materials is given. Third, the setup of the cured carbon fiber plate experiment is given. Fourth, the mode frequencies and mode shapes of the cured carbon fiber plate are presented and discussed. Fifth, a brief background of previous tennis racket research along with the tennis racket experiment setup is presented. Sixth, the effects of vibration dampers on the mode frequencies and mode shapes of a tennis racket is shown and discussed. Finally, a short conclusion is presented in order to review the important information gathered in this project.

2: Speckle-Pattern Interferometry Theory and Setup

Speckle-pattern interferometry represents a relatively low cost, real time method for measuring the vibrations of various surfaces. Moore, Lokberg, and Rosvold present generally equivalent, though differently phrased, overviews of the theory involved in SPI [9 – 13]. However, for the purposes of this paper, an overview of the theory involved is presented. The speckle-pattern interferometry setup used in these experiments can be found in Figure 1.

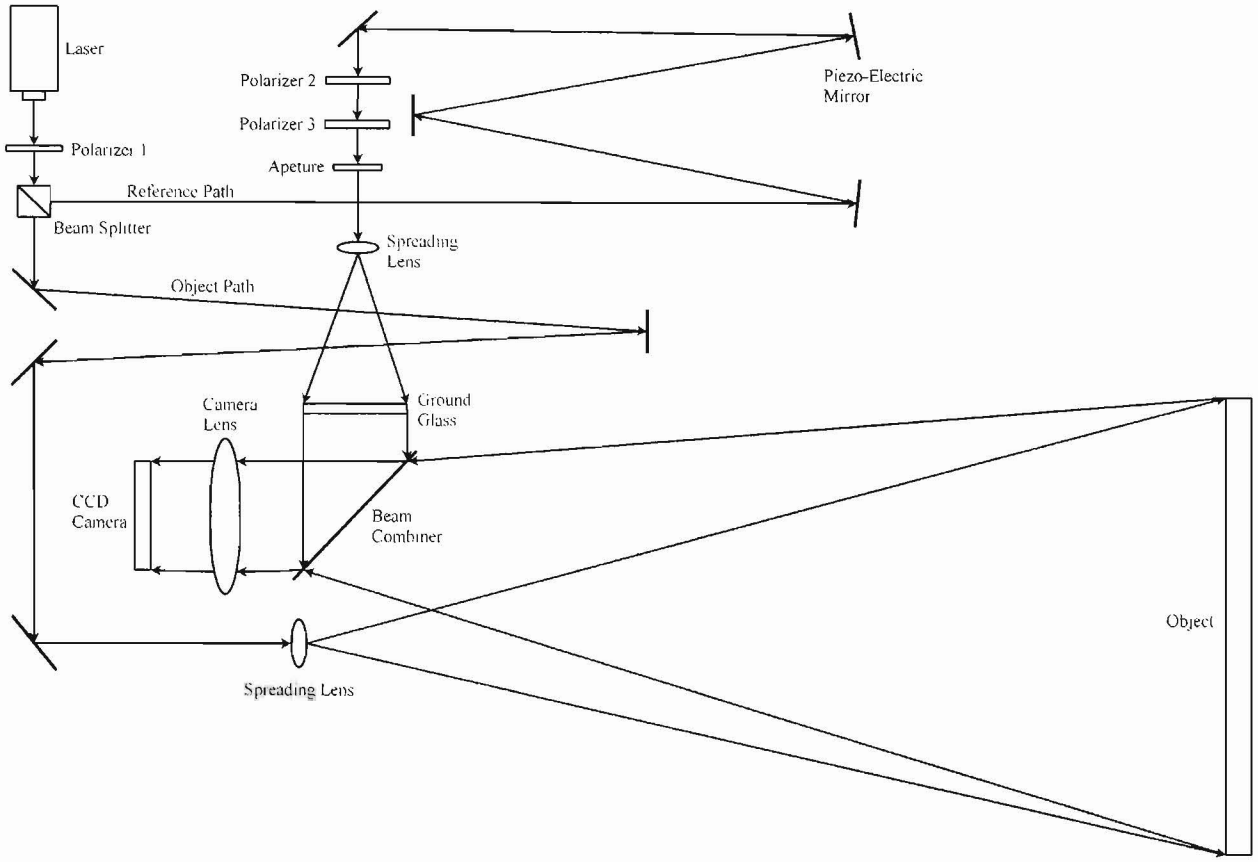

Figure 1: Speckle-Pattern Interferometry Setup

A laser beam (in this case a 532 nm HLaser OptoTech) is divided by a beam splitter into a reference and object beam. The object beam strikes an object and is partially reflected into a camera. The reference beam is directed to the camera through a beam splitter that serves to recombine the object and reference beams. In order to achieve interference between the object and reference beams, the beams must be coherent. The length of the reference beam path is held as close as possible to the object beam path length in order to maintain spatial coherence. The spatial coherence length for this laser is approximately 2 cm.[2] Also, in order to maintain polarization coherence polarizers one, two, and three are adjust such that the object beam and the

[2] The spatial coherence length of the laser was measured by Alex Boecher using a Michelson interferometer.

reference beam have the same polarization when recombined. In order to minimize background vibrations from the floor and maintain a stable optical setup, the entire system is placed on a Newport RS 4000 floating optical table.

In the classic speckle-pattern interferometry setup the optics of the object and reference paths are designed so that both beams appear to emerge from the exit pupil of the imaging lens system of the camera and therefore have the same divergence at the CCD [9]. However, in this experiment we utilize an interferometer design introduced by Moore that allows for simplification of the optics involved [9]. In this design, the complex optics surrounding the beam combiner is replaced by two elements: a piece of ground glass in the reference path immediately preceding the beam combiner and a commercial camera lens attached to the CCD camera. These changes do not alter the behavior of the interferometer while greatly simplifying the optical setup.

Speckle-pattern interferometry, as the name suggests, relies upon an interesting phenomena of coherent laser light, so called "laser speckle." When coherent laser light strikes a rough surface, the light reflects in many directions due to the roughness of the surface. The reflected light interferes with itself and produces the appearance of speckles on the surface of the material. This phenomenon can be seen in Figure 2 below.

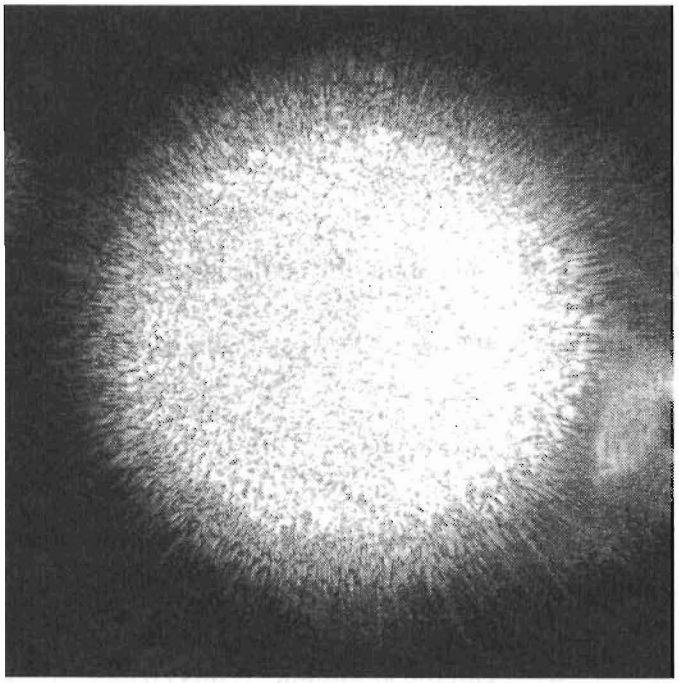

Figure 2: A Demonstration of Laser Speckle [14]

In order for maximum contrast to be obtained in the interferograms of vibrating objects, the average speckle diameter should be equal to the size of a pixel used to image the vibrating plate. The average speckle diameter is given by:

$$d \approx 1.22(1+M)\lambda F \qquad (1)$$

where M is the magnification and F is the focal ratio of the C-mounted zoom lens [9]. For our system M was measured to be approximately $9*10^{-3}$ and F was set to 7. Therefore, our average speckle diameter is approximately 5 μm. The pixel size of the CCD camera (Unibrain Fire-I firewire) is 5.4 μm. Thus, the speckle size and the pixel size were nearly identical, and therefore, a high degree of contrast was obtained with our system

When using speckle-pattern interferometry, an image is taken of the object prior to the onset of vibration. Then a second image is taken once the vibration has begun and transient behavior has ceased. These two images are subtracted, resulting in an interferogram. Assuming

the size of a pixel is approximately equal to the size of a speckle, the irradiance of a single pixel is given by the following:

$$I = I_o + I_r + 2\sqrt{I_o I_r}\cos(\theta) \tag{2}$$

where I_o is the irradiance of the object beam at the camera, I_r is the irradiance of the reference beam at the camera, and θ is the phase angle between I_o and I_r. Thus, prior to the onset of vibration, the irradiance I_1 is given by:

$$I_1 = I_o + I_r + 2\sqrt{I_o I_r}\cos(\theta_0) \tag{3}$$

where θ_0 is the original phase difference. As the object vibrates, the position of the points on the object change slightly in the z-axis, call the amplitude of this change Δz, such that the phase angle becomes:

$$\theta = \theta_0 + \xi\sin(\omega_0 t) \tag{4}$$

where ω_0 is the angular frequency of vibration of the object and ξ is given by:

$$\xi = \frac{2\pi\Delta z}{\lambda}[\cos(\theta_i) + \cos(\theta_r)] \tag{5}$$

where λ is the wavelength of laser light used to illuminate the object, θ_i is the incident angle of the object beam measured normal to the surface, and θ_r is the reflection angle of the object beam measured normal to the surface.

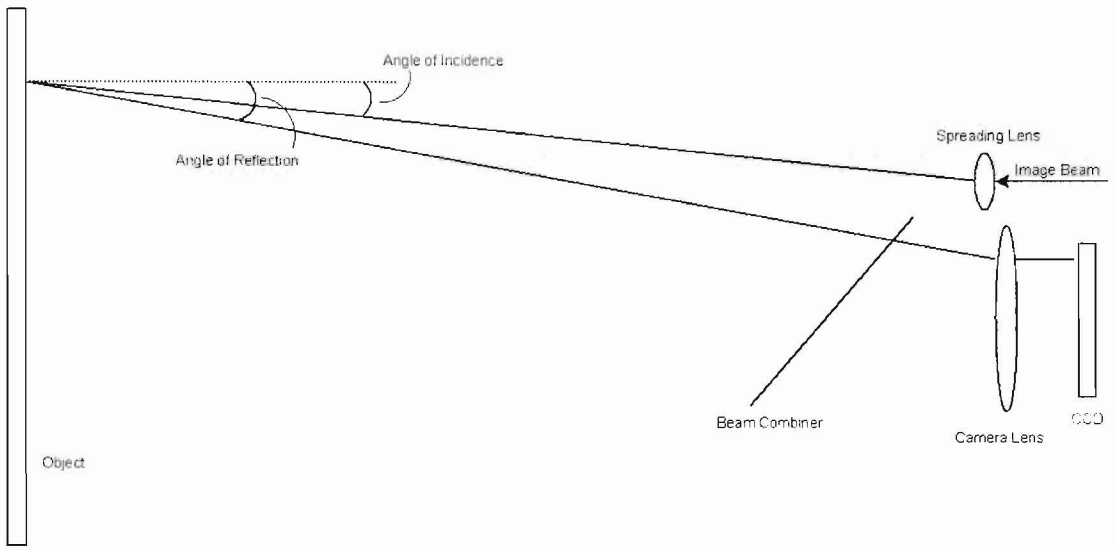

Figure 3: Incident and reflection angles from the object

In the setup employed θ_i and θ_r are small, such that $(\cos(\theta_i)+\cos(\theta_r))\geq 1.98$. Thus, ξ can be approximated as:

$$\xi \cong \frac{4\pi\Delta z}{\lambda} \tag{6}$$

Thus, when undergoing vibration the irradiance of a pixel is given by:

$$I_2 = I_o + I_r + 2\sqrt{I_o I_r}\cos(\theta_0 + \xi\sin(\omega_0 t)) \tag{7}$$

The frame rate of the camera is approximately 10 fps. In order to insure that the integration time of the camera is significantly longer than the period of vibration of an object, we restricted our observations to objects vibrating at frequencies greater than 30 Hz. So, an image of the object undergoing vibration is an average of I_2 and is given by [9, 12, 13]:

$$\bar{I}_2 = I_o + I_r + 2\sqrt{I_o I_r}J_0(\xi)\cos(\theta_0) \tag{8}$$

where J_0 is the zero-order Bessel function of the first kind.

Traditionally, the interferogram would be produced by taking the absolute value of the difference between $\bar{I}_2$ and I_1. However, this method can be problematic due to speckle

decorrelation over the time it takes between the two images. Every attempt has been made to minimize speckle decorrelation with the use of a vibrationally isolated optical table and sturdy clamping of the object mount to the optical table, but decorrelation does occur. In fact, early tests of the setup employed showed decorrelation effects after as short as 3 seconds. Therefore, instead of taking one image prior to vibration and subtracting it from an image taken during vibration, successive images are taken during vibration are subtracted to form the interferogram. This process is accomplished with a LabVIEW program.[3]

Let the successive images taken while the object is vibrating be denoted as image m and image n. Again, each image is an average, so $\bar{I}_m$ and $\bar{I}_n$ are given by:

$$\bar{I}_m = I_o + I_r + 2\sqrt{I_o I_r} J_0(\xi)\cos(\theta_m) \tag{9}$$

$$\bar{I}_n = I_o + I_r + 2\sqrt{I_o I_r} J_0(\xi)\cos(\theta_n) \tag{10}$$

where θ_m and θ_n are the respective phase angles of these images. When image n is subtracted from image m and the absolute value is taken, the result for the irradiance of a given pixel on the interferogram mn is given by:

$$I_{mn} = \left|2\sqrt{I_o I_r} J_0(\xi)(\cos(\theta_m) - \cos(\theta_n))\right| \tag{11}$$

As can be seen from equation (11), if $\cos(\theta_m) = \cos(\theta_n)$ then the interferogram mn will be completely black and no useful information will have been gained. In order to insure that $\cos(\theta_m) \neq \cos(\theta_n)$, a slow (~1 Hz) linear variation in the phase angle is introduced by the placement of a mirror attached to a piezo-electric disk in the reference path [15]. The piezo-electric mirror was controlled by a Agilent 33220A signal generator.

[3] The LabVIEW program used has undergone many iterations and improvements. This work has been accomplished by numerous individuals over several semesters: Andrew Morrison, Tim Boecher, Tom Traynor, Kristy Streu, Tom Moore (Rollins College), and Sawyer Campbell.

From (11) and (6), it is apparent that in nodal regions I_{mn} will be maximized since $J_0(0)=1$. As Δz increases from 0, $|J_0(\xi)| \to 0$ ($|J_0(\xi)|=0$ at $\xi \approx 2.4$). Hence, the vibrating regions adjacent to nodes will appear black in interferograms. As ξ increases from approximately 2.4, $|J_0(\xi)| \tilde{\to} .4$. Therefore, another bright region should be present in vibrating regions. This process will continue to cycle through bands of black and white with decreasing brightness as the Bessel function approaches 0 (these bands are referred to as "fringes"). The relationship between the appearance of nodes and fringes and the mathematical behavior of the Bessel function can be seen in Figure 4.

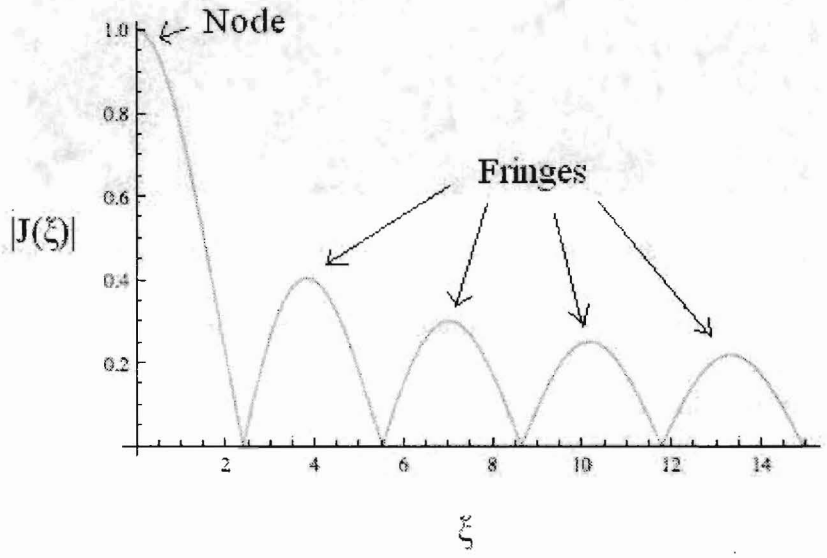

Figure 4: The absolute value of a zero-order Bessel function of the first kind.

An example of this behavior can be seen in Figure 5.

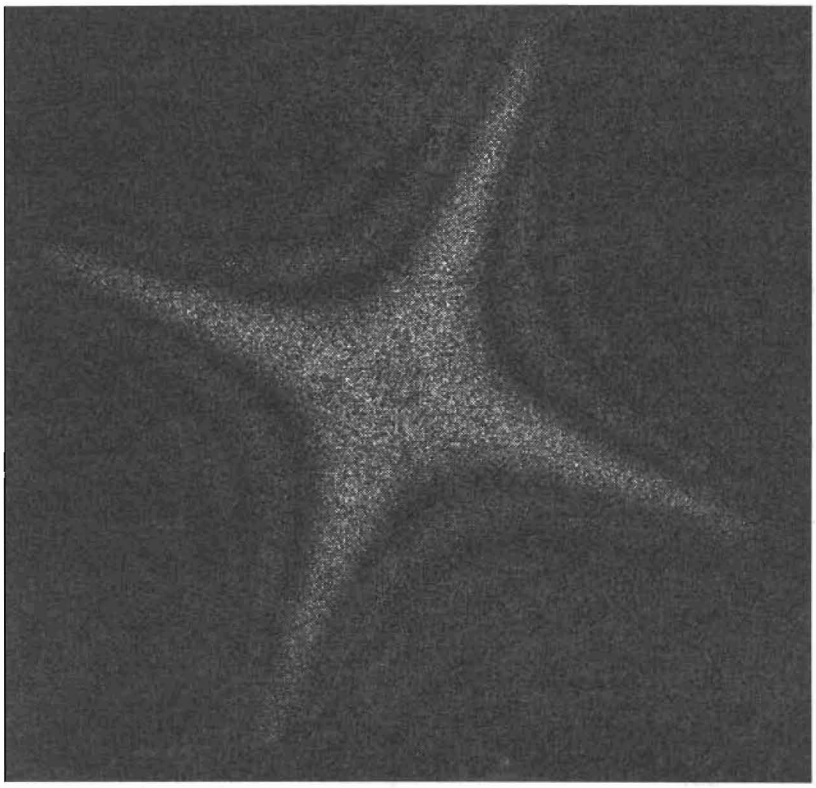

Figure 5: An example interferogram of a steel disk supported at its center vibrating at 167 Hz.

In Figure 5 bright nodes form a cross in the middle that corresponds to $J_0(0)=1$. In the regions between the arms of the nodal cross the alternating black-white banding structure is seen that indicates displacement. As the displacement grows larger near the edge of the disk the intensity of the bright bands decreases as was predicted by the behavior of the Bessel function. Generally, as the fringe density increases, the vibrational amplitude also increases.

3: The Vibrational Behavior of a Cured Carbon Fiber Disk

3.1: Orthotropic Material Background and Setup

An orthotropic material possesses different material properties in orthogonal directions. A classic example of this type of material is wood. The Young's Modulus and other material properties differ in the direction of the grain compared to those material properties in the

direction perpendicular to the grain. In this project, the orthotropic material under consideration is cured carbon fiber plate which represents a unique type of orthotropic material.

In order to understand the structure of cured carbon fiber plate, it is necessary to provide a general overview of the carbon fiber plate manufacturing process [16, 17]. First, a material with high carbon content undergoes successive baking procedures and is then extruded in order to produce long carbon fibers. The three most common base materials from which carbon fiber is constructed are viscose rayon, pitch, and polyacrylonitrile $[(CH_2CHCN)_n]$. These carbon fibers are then spun to form carbon fiber thread. This thread is then woven in *perpendicular* directions to form a flexible carbon fiber sheet. Finally, the sheet is cured, or hardened, using some type of binder such as polyester or epoxy resin. The important point of note in the construction of cured carbon fiber plate is that the carbon fibers within the plate are woven in perpendicular directions. Thus, the material properties of carbon fiber are anisotropic since they depend upon direction. The material properties are identical in orthogonal directions, so technically cured carbon fiber plate may be considered to be only anisotropic and not orthotropic. That said having been said, the material construction seems to imply that carbon fiber plate should be treated as an orthotropic material. For this reason, carbon fiber plate is difficult to classify, especially in terms of the appropriate vibrational behavior theory to apply. However, the material properties of one set of orthogonal directions are different from the material properties of any other distinct set of orthogonal directions. Because of this, for the purposes of this paper and with regards to theory, cured carbon fiber plate will be considered an orthotropic material with identical properties in orthogonal directions.

In this project, the vibrational behavior of a circular cured carbon fiber disk was examined using the speckle-pattern interferometry system discussed above. The disk was

originally order as a 1' by 1' square with a thickness of 1/32". It was purchased from McMaster Carr, part number 8181K12.

The plate was cut into a circle of radius 28 cm and had a small hole drilled at its center. The plate was then mounted by way of a bolt through the center hole to a heavy post that was positioned on the optical table. The disk was sprayed with a thin coat of Chase Products' Santa SnowFrost, a commercial available false frost that increased the reflectivity of the black carbon fiber immensely. Also, the false frost provided a nearly uniform roughness, which in turn produced a nearly uniform speckle size. For these reasons all objects studied using the speckle-pattern interferometer were sprayed with the false frost. The disk and its mounting apparatus can be seen in Figure 6.

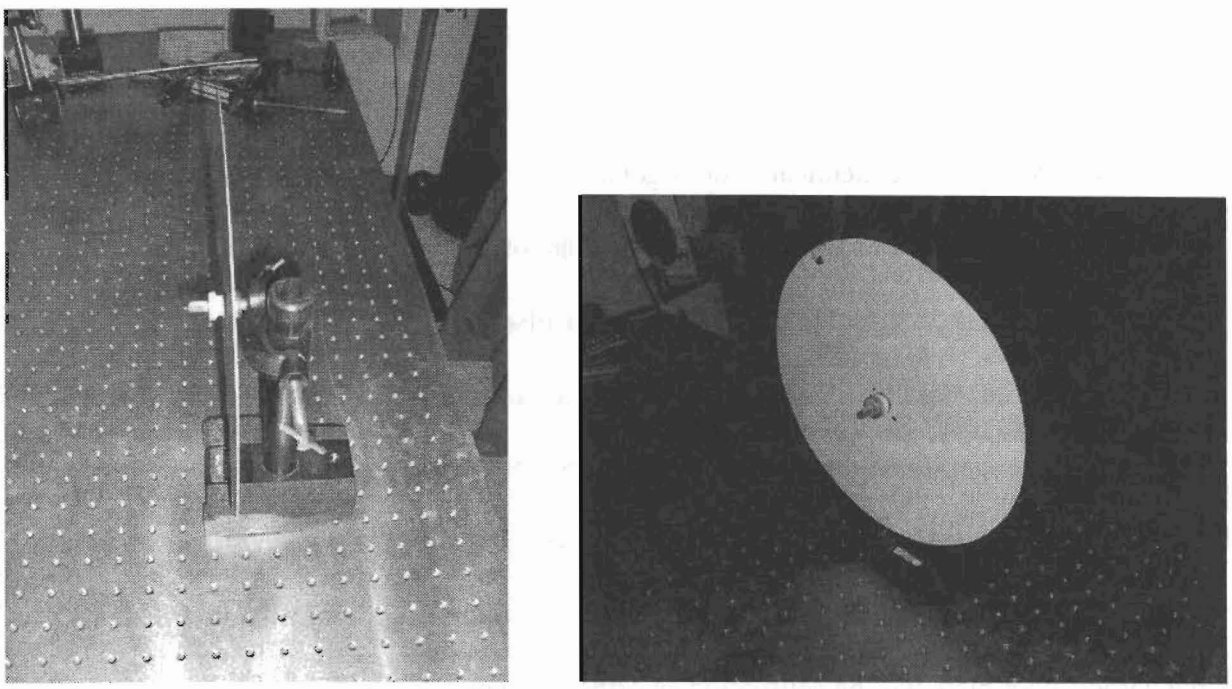

A B

Figure 6: The circular cured carbon fiber plate disk attached to its mounting structure. A) view from profile, B) view from front

The disk was vibrated by attaching a small magnet to the reverse side of the disk. The magnet was vibrated by locating a solenoid nearby and placing an alternating current through the solenoid. The alternating current was produced by a Hewlett-Packard 3325A Signal Generator and controlled by a LabView program.[4] In this way, it was possible to apply a specific frequency and amplitude vibration to the carbon fiber plate. Generally, vibrating an object acoustically is preferable to using a magnet and solenoid because the added mass of a magnet affects the vibrational behavior of the object. Some of these effects will be discussed below in sections 3.3 and 3.4. An object is vibrated acoustically using a specific frequency sound wave generated by a speaker placed near the object. However, it was found that the disk was difficult to vibrate precisely with the acoustical method, so the magnet and solenoid method was employed.

3.2: Mode Nomenclature

The vibrational behavior of an isotropic disk has been thoroughly studied during the past two centuries [1, 18 – 25]. The mode shapes of a vibrating isotropic disk supported at its center can be seen in Figure 7.

[4] This program was designed by Sawyer Campbell and Alex Boecher

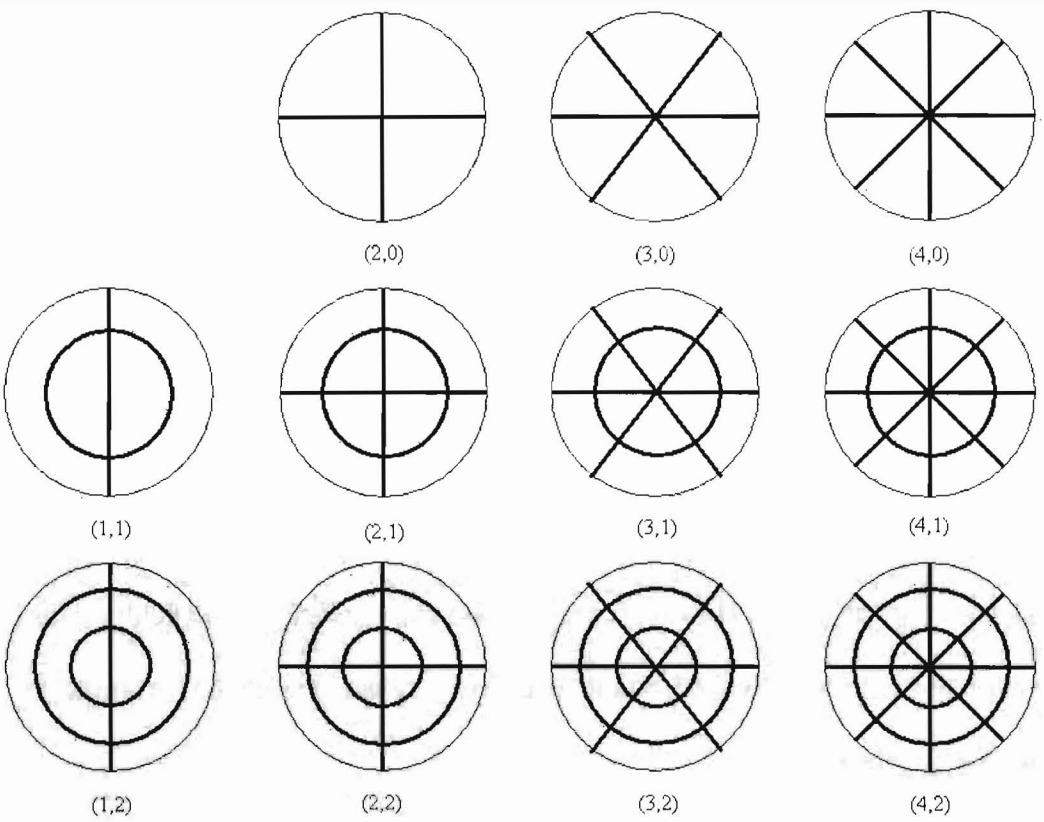

Figure 7: The first few mode shapes of an isotropic disk support at the center [1]. The bold lines indicate nodes while the light edge ring merely indicates the edge of the plate.

The modes of a vibrating circular disk are denoted by the number of nodal diameters and nodal circles. For instance, mode (2,0) possesses two nodal diameters and zero nodal circles, while mode (3,1) possesses three nodal diameters and one nodal circle. The (2,0) is the fundamental mode for this boundary condition. Generally speaking, the mode frequency increases with the increase in the number of nodal diameters and nodal circles.

3.3: Modal Frequencies

The determination of mode frequency followed a two step process. First, the plate was gently tapped in order to induce vibration. A short impulse effectively inputs a wide range of frequencies. The object responds to this input by vibrating most at its modes or resonant frequencies. These vibrations then radiate sound waves which were measured using a sound level

meter connected to a Ono Sokki CF-920 spectrum analyzer. The spectrum analyzer then performs a fast Fourier transform in order to produce a frequency spectrum. Amplitude peaks in the frequency spectrum usually correspond to modes. The speckle-pattern interferometer was then used to take several interferograms near the target frequencies identified using the spectrum analyzer in order to confirm the frequencies found using the spectrum analyzer were due to resonances and not due to particularly dominant mixed modes. The geometry of the mode shapes of the disk are well known, so identifying modes using the speckle-pattern interferometer is relatively easy. In addition, mode frequencies and mode shapes are identified using the speckle-pattern interferometer by imaging large amplitude vibrations, or resonances, at modes.

As was stated previously, classifying carbon fiber as orthotropic is technically incorrect, but the construction of carbon fiber implies an orthogonal treatment in which the material properties in perpendicular directions are identical. However, in the case of the theory developed by Rossing, the theory for orthogonal materials in which material properties are identical in perpendicular directions reduces to the theory for isotropic materials [1]. The mode frequencies of an isotropic plate supported at its center can be expressed as ratios related to the fundamental mode ((2,0)) frequency [1]. The (2,0) mode frequency is given by:

$$f_{20} = \frac{0.2413 c_L h}{a^2} \tag{12}$$

where c_L is longitudinal speed of sound in the material, h is the thickness of the plate, and a is the radius. The longitudinal speed of sound of a material is given by:

$$c_L = \sqrt{\frac{E}{\rho(1-\nu^2)}} \tag{13}$$

where E is Young's modulus, ρ is the density, and ν is Poisson's ratio. The relative mode frequencies of an isotropic disk supported at its center can be found in Table 1.

Mode	Mode Freq. / f(2,0)
(2,0)	1
(3,0)	2.328
(4,0)	4.11
(5,0)	6.3
(1,1)	3.91
(2,1)	6.71
(3,1)	10.07
(4,1)	13.92
(5,1)	18.24
(1,2)	11.4
(2,2)	15.97
(3,2)	21.19
(4,2)	27.18
(5,2)	33.31

Table 1: Expected mode frequencies of an isotropic plate supported at its center. [1]

According to Rossing, for orthotropic plates, only c_L is influenced by the orthotropic nature of a material [1]. Thus, the ratios between the mode frequencies of any orthotropic plate (including the case of materials with identical properties in perpendicular directions) should remain identical to the ratios between the mode frequencies of an isotropic plate.

The mode frequencies observed for a carbon fiber disk supported at its center can be found in Table 2.

Mode Number (m,n)	Frequency (Hz)	f(m,n)/f(2,0)	Expected f(m,n)/f(2,0)	% Diff.
(2,0)	72	1	1	0
(1,1)	250	3.5	3.91	11
(2,1)	364	5.0	6.71	29
(1,2)	707	9.8	11.40	15
(2,2)	795	11	15.97	37
(2,2)	895	12	15.97	28
(3,2)	1062	15	21.19	34

Table 2: Observed mode frequencies of a carbon fiber disk supported at its center.

The mode frequencies observed for the carbon fiber disk are quite different from those predicted by Rossing. Furthermore, the percent differences between the expected and observed frequency

ratios vary greatly between modes. Most importantly, the measured ratios are consistently below the expected ratio. This consistency implies that the large percent differences are not only due to random error. We feel that these large percent differences imply that the theory presented by Rossing does not apply to this system. Perhaps classifying the cured carbon fiber plate as orthotropic with identical material properties in orthogonal directions is incorrect and doing so leads to the inapplicability of Rossing's theory. In any case, it is clear that a new theoretical approach must be made to understand the mode frequencies of carbon fiber plate.

As can be seen in Table 2, the (2,2) mode is listed at two frequencies. This double frequency is due to the presence of split degenerate mode shapes. In some systems, more than one distinct mode shape exists for certain mode frequencies [26]. For instance, in the case of a square plate clamped at all edges, the second mode possesses a nodal line from one edge to the opposite edge. However, in this case nothing determines whether the nodal line is from the top edge to the bottom edge or from the left edge to the right edge. Thus, this mode is degenerate since it possesses two distinct mode shapes that vibrate at the same mode frequency. These mode shapes can be seen in Figure 8.

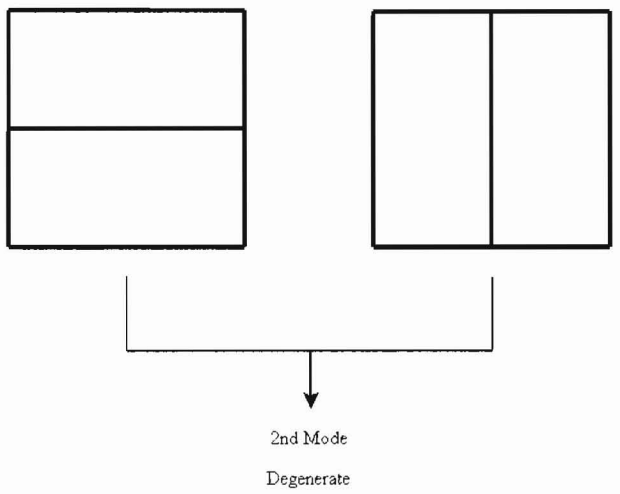

Figure 8: Degenerate second mode of a square plate clamped on all sides. All lines are nodes.

In the case of the carbon fiber disk, it may be thought that the method of vibration split the degeneracy of the (2,2) mode. The presence of the magnet on the disk added a small, but not insignificant, mass to the disk. Therefore, if the mass is located near an anti-node of one of the degenerate shapes, that degenerate mode shape will appear at a lower frequency since it takes more energy to vibrate the extra mass. If the mass is located near a node of one of the degenerate shapes, that degenerate mode shape will appear at a higher frequency since the mass does not have to vibrate much in the production of that mode shape. However, in the case of our setup, the mass of the magnet was very small compared to the mass of the disk. The mass of the magnet and the adhesive used to join the magnet to the disk was approximately 0.14 g. The mass of the disk is approximately 76.49 g. Therefore, the mass of the vibrating system increased by only approximately 2% by adding the magnet, yet the split degenerate modes were separated by approximately 100 Hz. Even speaking roughly this is a much larger split than expected. For instance, the frequency of a harmonic oscillator is proportional to $(\text{mass})^{-(1/2)}$. Thus, increasing the mass by 2% should only lower the frequency by $\sqrt{2}$ %, or in this case, approximately 1 Hz. The large disparity between the rough approximated frequency split and the observed frequency split is certainly noteworthy. Further unexpected behavior was be seen with regards to the mode shapes of the degenerate (2,2) mode.

3.4: Mode Shapes

Interferograms of the mode shapes of the carbon fiber disk were taken using the speckle-pattern interferometer. In addition, interferograms of the mode shapes of an isotropic steel disk were also taken for comparison. The steel disk was mounted in the same fashion as the carbon fiber disk and it had the same radius. The material properties of the metal disk are unknown.

However, the steel disk is isotropic, which is all that is necessary in order to perform a meaningful comparison between isotropic and orthotropic disk mode shapes.

As was stated above, the carbon fiber disk was vibrated using a magnet fixed to the reverse side of the disk. Two magnet positions were utilized in order to better understand the role of the magnet location in the mode shape. Magnet position A was approximately 1 cm left and 3 cm below the center. Magnet position B was approximately 3 cm left and 1 cm below the center. The magnet position is indicated with a red point in the interferograms Also, the weave, or ply, orientation is rotated approximately 45 degrees from the horizontal and vertical axes. The weave axes are indicated in interferograms with blue perpendicular lines.

An interesting flattened nodal circle shape can be seen in the mode shapes of the (2,1) and (1,1) modes.

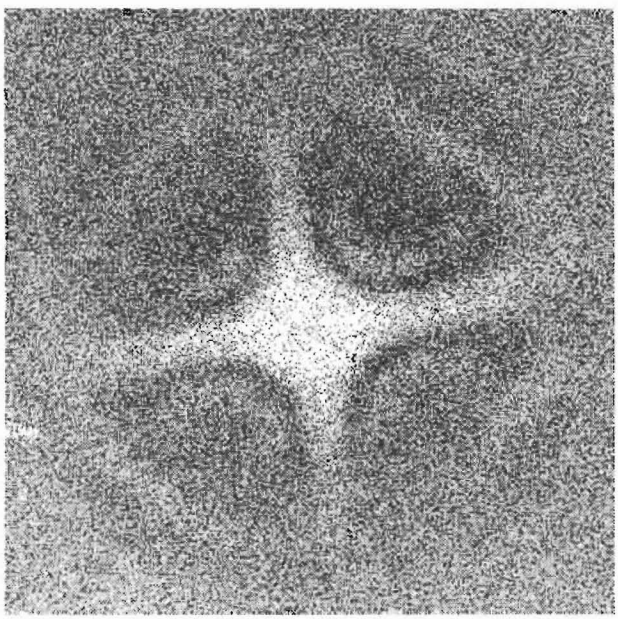

A

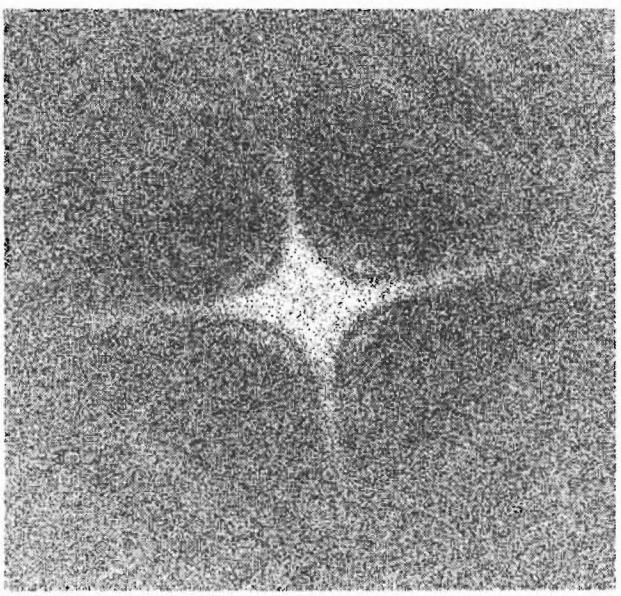

B

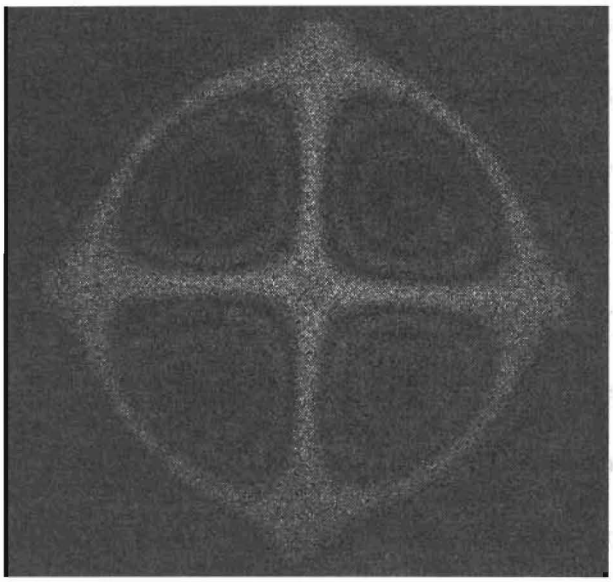

C

Figure 9: (2,1) Mode: A) Carbon Fiber Plate Magnet Position A 364 Hz, B) Carbon Fiber Plate Magnet Position B 363 Hz, C) Steel Plate 1023 Hz

In Figure 9 we see that the nodal circle in the carbon fiber disks is somewhat flattened. Also, the nodal diameters appear to be rotated approximately 45° with respect to the weave orientation. In comparison, the nodal circle of the (2,1) mode of the steel disk is not flattened. A similar behavior was observed in the mode shapes of the (1,1) mode.

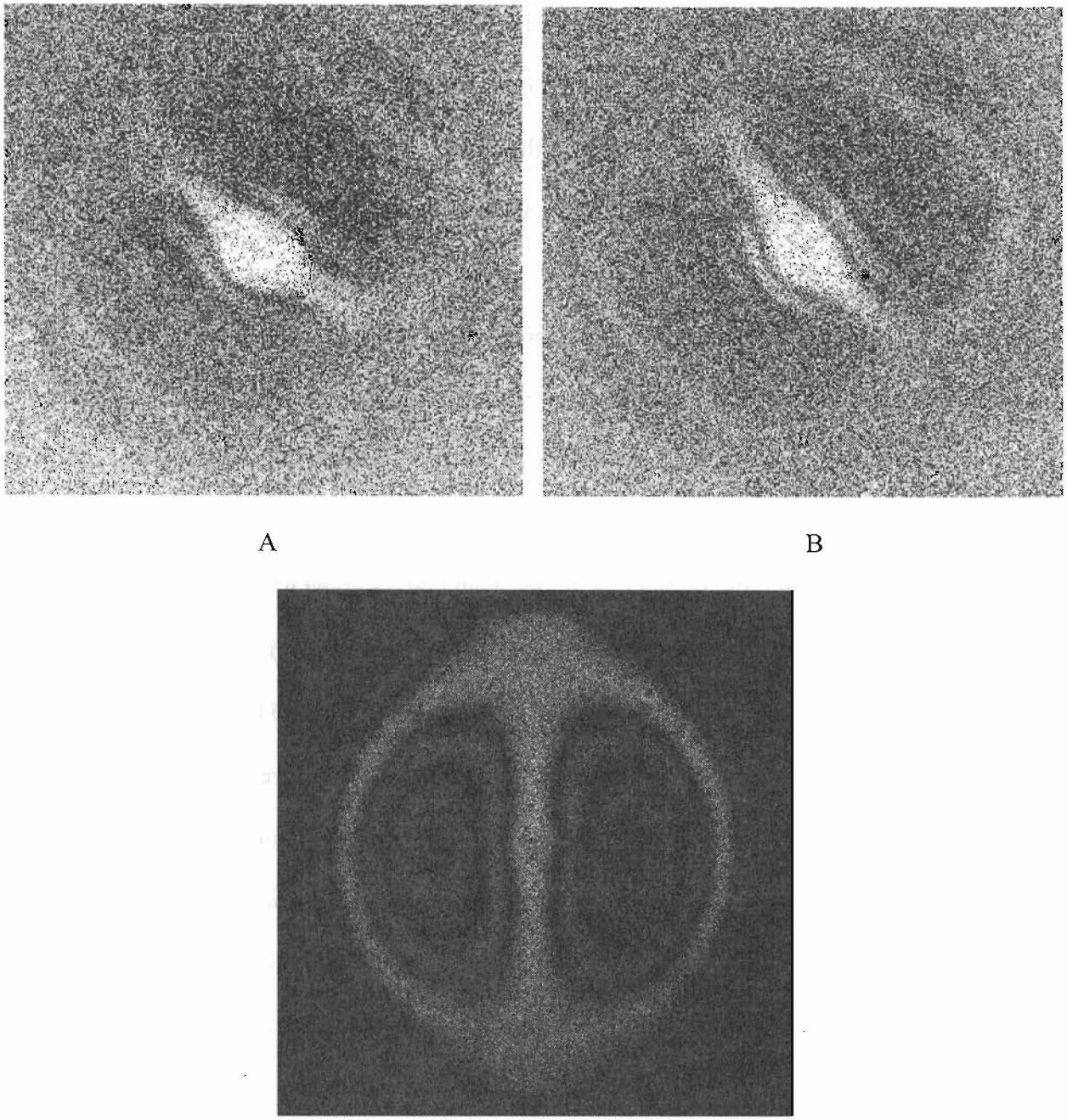

A B

C

Figure 10: (1,1) Mode: Top) Carbon Fiber Plate Magnet Position A 250 Hz, Middle) Carbon Fiber Plate Magnet Position B 250 Hz, Bottom) Steel Plate 652 Hz

Again, in Figure 10 a definite flattened circle shape can be seen with regards to the nodal circle in the carbon fiber plate that is conspicuously absent in the steel plate's nodal circle. Also, the nodal diameter appears to be rotated approximately 45° with respect to the weave orientation.

The flattened nodal circle and rotated nodal diameter phenomena were also observed for the higher split degenerate (2,2) mode (~895 Hz), but interestingly was not observed for the lower mode (~795 Hz). For magnet position B, the higher split mode exhibited a flattened nodal circle and a nodal diameter rotation of approximately 45 degrees with respect to the weave orientation (Figure 11 B). For magnet position A, the higher split mode (~895 Hz) exhibited a nodal diameter rotation of approximately 45 degrees with respect to the weave orientation and a somewhat flattened nodal circle, though not as prominently as was seen in magnet position B (Figure 11 A). These degenerate modes were observed with the magnet positioned near an anti-node. However, if the split degeneracy had been due to the added mass of the magnet, it would have been anticipated that these degenerate modes would be observed with the magnet positioned near the node. With regards to the lower split degenerate (2,2) mode, the square nodal circle behavior was not apparent and the weave orientation was observed to be in the same direction as the nodal diameters for both magnet position A and B (Figure 11 C and D). Also, the lower frequency degenerate mode was observed with the magnet positioned near the nodal diameter. However, if the split degeneracy had been due to the added mass of the magnet, it would have been anticipated that the lower split mode would have the magnet positioned in the anti-node. The fact that the degenerate states split in the opposite fashion as would have been expected had the split been due to the added mass of the magnet and the fact that the frequency difference between the two split mode shapes is so large leads to the conclusion that the split degeneracy seen in the (2,2) mode is not due to the added mass of the magnet. No degeneracy or square nodal circle phenomena were observed for the (2,2) mode shape of the steel disk (Figure 11 E).

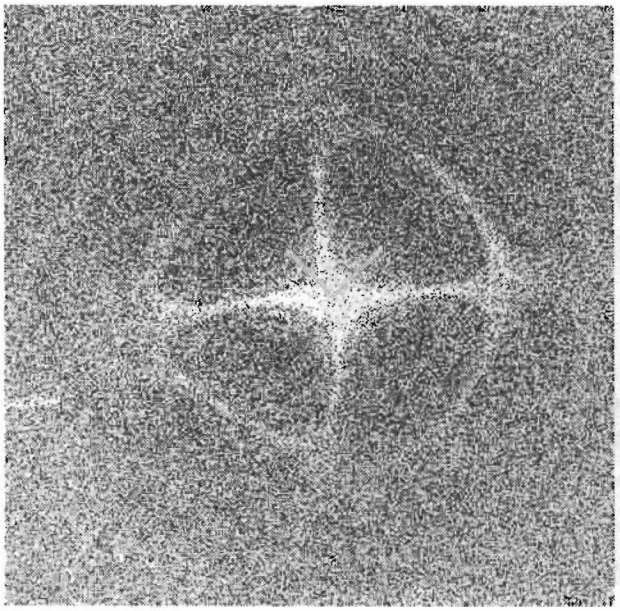

A

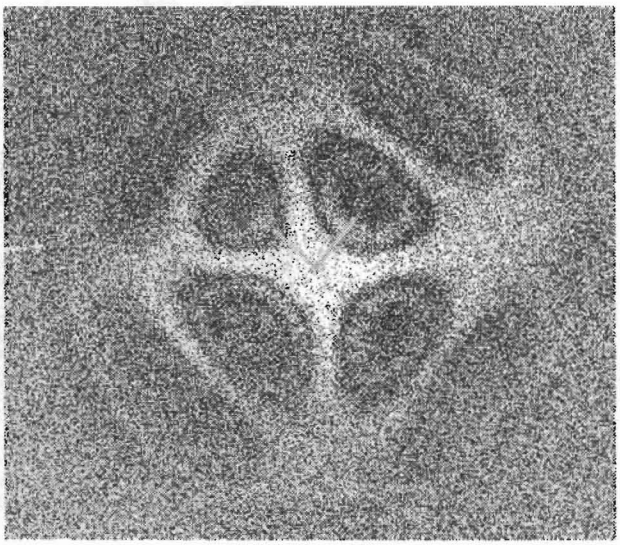

B

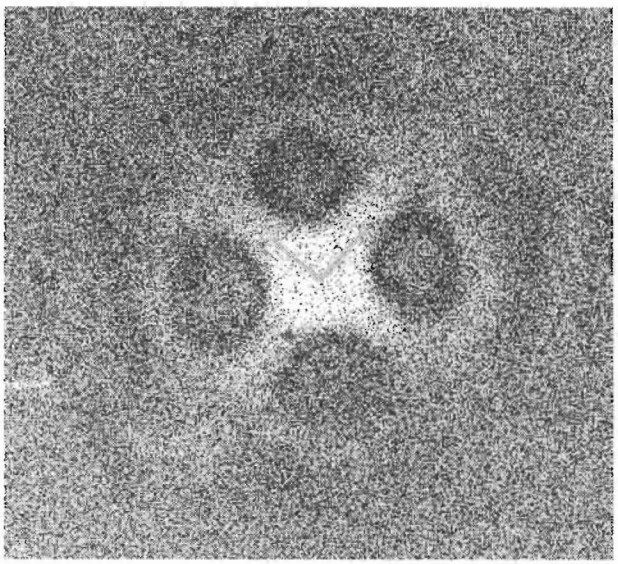

C

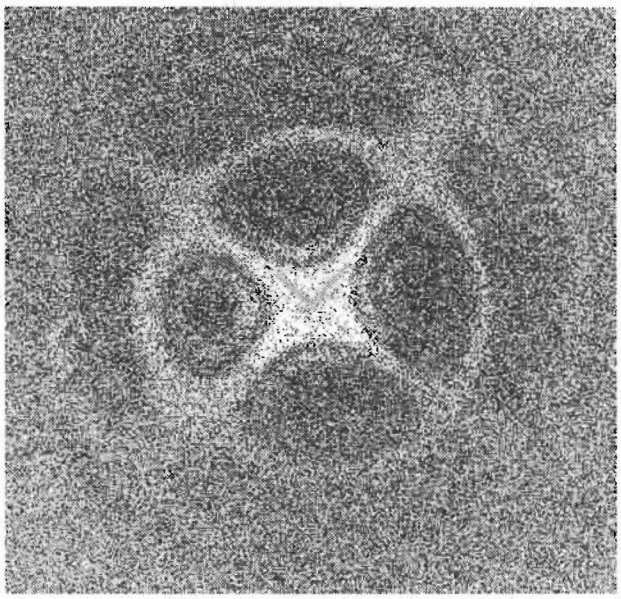

D

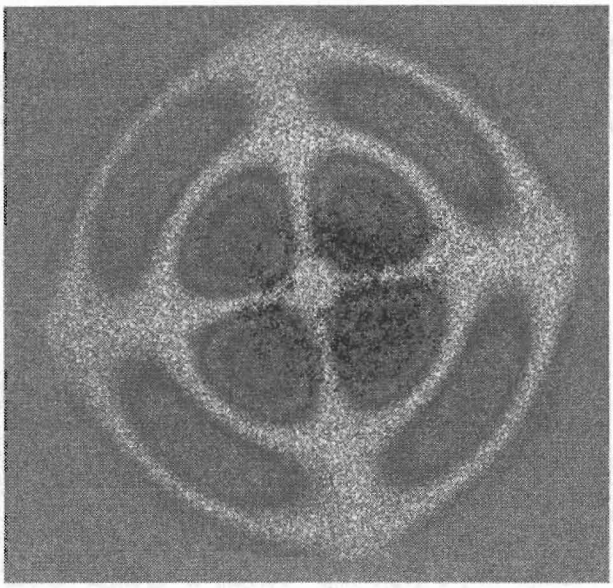

E

Figure 11: Split Degenerate (2,2) Mode Shapes: A) Magnet Position A 892 Hz, B) Magnet Position B 897 Hz, C) Magnet Position A 800 Hz, D) Magnet Position B 791 Hz, E) Steel Disk 2446 Hz

The vibrational behavior of the carbon fiber disk appears to point to a few possible principles. The two stable positions for the orientation of the nodal diameters are aligned with the weave direction and rotated 45° with respect to the weave orientation. Also, in some circumstances, the nodal circles exhibit a square behavior. However, this behavior is not consistent. Both of these phenomena may be influenced by the magnet position, the orthogonal construction of the plate, or both. In addition, the carbon fiber plate exhibited unexpected degeneracy behavior. The degenerate (2,2) mode was split by an unexpectedly large frequency and this phenomena can not be accounted for with the added mass of the magnet. In order to better understand the influence of the orthogonal construction of carbon fiber we should study this disk with more attention to the magnet position. Also, it would be necessary to study other plate setups and boundary conditions. For instance, a square plate clamped at it edges should be studied along with a circular plate clamped at its edges.

4: The Vibrational Behavior of a Tennis Racket

4.1: Background and Setup

A great deal of research has been performed concerning the mechanical behavior of the tennis racket [27 – 32]. The purpose of this project with regards to tennis rackets was two fold: to observe the vibrational behavior of a tennis racket using the speckle-pattern interferometry system described above and to test the effects of various commercially available vibrational damping systems on the vibrational behavior of a tennis racket. While some publications have discussed specifically the vibrational behavior of the tennis racket [33, 34], as far as the author is aware, no one has employed speckle-pattern interferometry to directly observe the vibrational behavior of a tennis racket. In addition, several authors have studied the effects of vibration dampers on the mechanical performance of the tennis racket [5 – 8], but again no one has directly observed the changes in vibrational behavior caused by vibration dampers. The vibration damping systems, of which there are several distinct designs, are advertised as lessening uncomfortable high frequency vibrations in the racket that lead to a bad "feeling" in the racket as experienced by the player. The purpose of this paper is not to directly assess the claimed performance of the vibration damping systems with regards to the feeling experienced by the player; rather the goal is to observe what effects, if any, these systems have on the mode shapes and vibrational amplitude of a tennis racket.

The following observations of the vibrational behavior of a tennis racket were performed using a Pro-Kennex Reach Precept 110 tennis racket. The racket was mounted to the optical table using two test tube clamps on magnetic post stands. As with the plates studied above, the tennis racket was sprayed with false frost. Due to the relatively low surface area of the tennis racket, the most efficient method of vibration was found to be the same method employed with the carbon

fiber disks. A small magnet was attached to the racket frame near the handle. The magnet was driven by an alternating current passing through a solenoid. This setup can be seen in Figure 12.

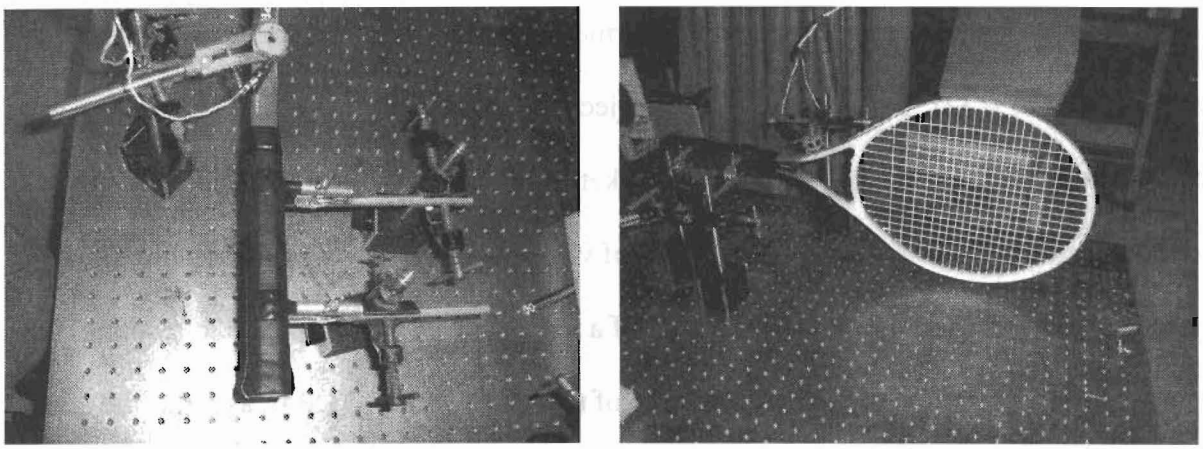

Figure 12: The tennis racket mounted to the optical table.

There has been some consideration in the literature regarding the proper method of attaching the racket to the table [35, 36]. For instance, Brody determined that the vibrational behavior of a rigidly clamped racket following the impact of a tennis ball is significantly different from the vibrational behavior of a hand held racket following the impact of a tennis ball [35]. Most importantly, Brody notes that the vibration decay time in the rigidly clamped racket is significantly longer than the decay times for a hand held racket and that several low frequency vibrations are not present following impacts with hand held rackets, while these vibrations are present following impacts with rigidly clamped rackets. Within this project, though, issues surrounding the very complicated physics of the ball-racket interaction will not be addressed. Furthermore, the physics involved in the racket-hand interaction are far too complicated to be addressed within this project. It was outside the scope of the project to build a clamping system that would accurately simulate the different pressures applied by the hand at the different points they are applied and the continuous variation of these pressures. Since this project is only concerned with the vibrational behavior of the racket and how the vibrational behavior is altered

by the presence of a vibration damper, clamping the racket to optical table rigidly was sufficient. It should be noted that the mounting system employed was not completely rigid in that the test tube clamps were covered in rubber and the racket handle is wrapped in a compressible tape.

In order to reduce uncertainty, all tennis racket interferograms were taken on the same day with no changes being made to the clamping system or the method of vibration. In addition, unless otherwise noted, all interferograms were taken with the same vibrational amplitude driving force applied to the racket. Constant driving vibrational amplitude was used in order to gain useful information about the vibrational amplitude. The relative vibrational amplitude can be measured by two methods. The size of the nodes indicates the relative vibrational amplitude in that small nodes accompany large vibrational amplitudes. Also, a large number of fringes indicates that the vibrational amplitude is large (see section 2). Thus, the size of nodes and regions of vibration in these interferograms conveys information about the relative vibrational amplitude of the modes between the undamped racket and the racket with the various vibration dampers in place.

4.2: Vibration Damping Systems

There are several vibration damping systems are commercially available today. In this project a sample of four such models were studied: the Wilson Vibra-Fun (specifically the rectangular model), the Prince NXG Silencer, the Head Smartsorb, and the Babolat RVS. All of these models cost around five dollars and claim to offer a low cost way to improve racket feel by diminishing uncomfortable high frequency racket vibrations. These models in their original packaging can be seen in Figure 13.

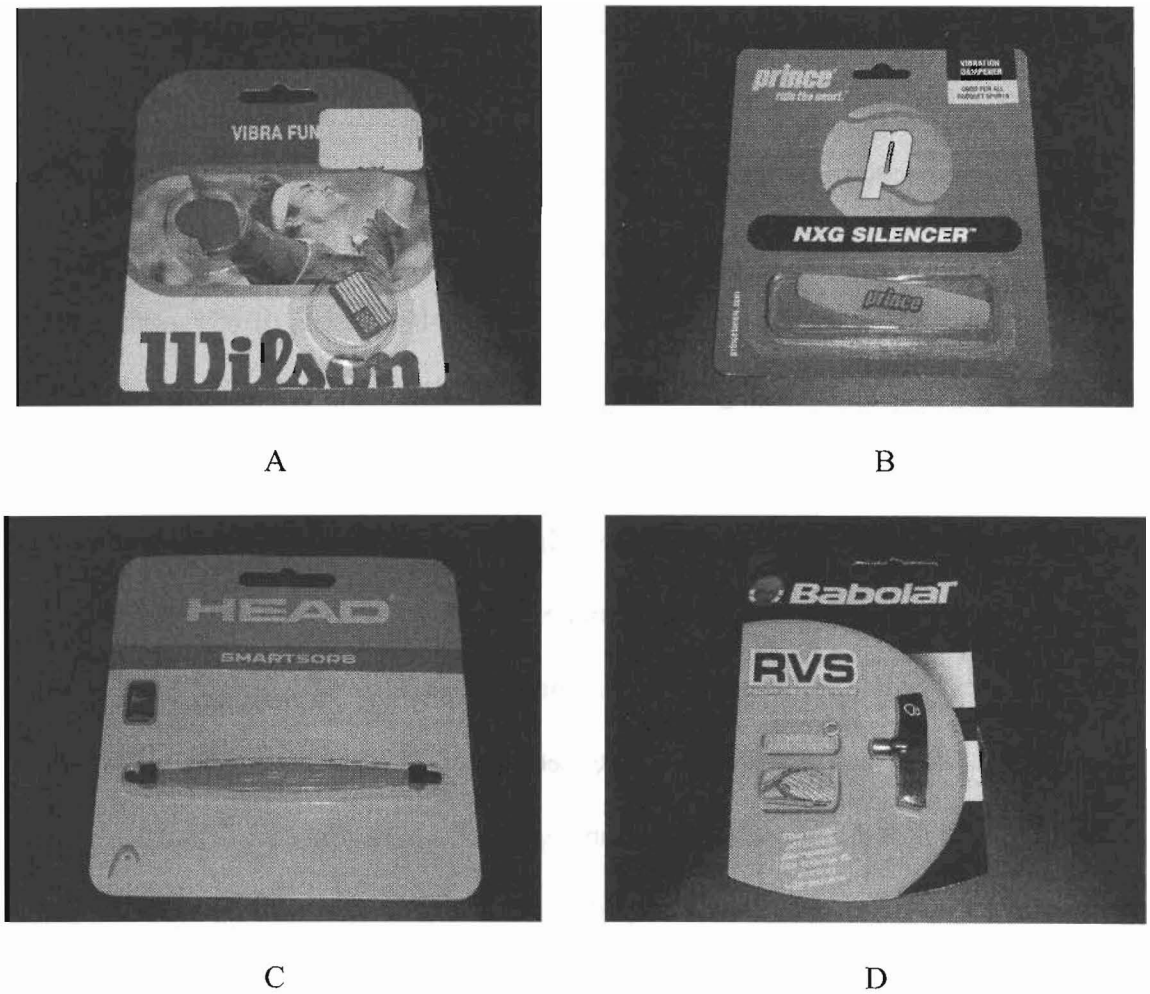

A B

C D

Figure 13: Vibration Damping Systems: A) Wilson Vibra-Fun (specifically the rectangular model), B) Prince NXG Silencer, C) Head Smartsorb, D) Babolat RVS

All four models of vibration dampers attach to the racket near the bottom of the racket head. All models supplied rudimentary directions about how to attach the device to the racket and these were followed explicitly. The dampers can be seen attached to the racket in Figure 14.

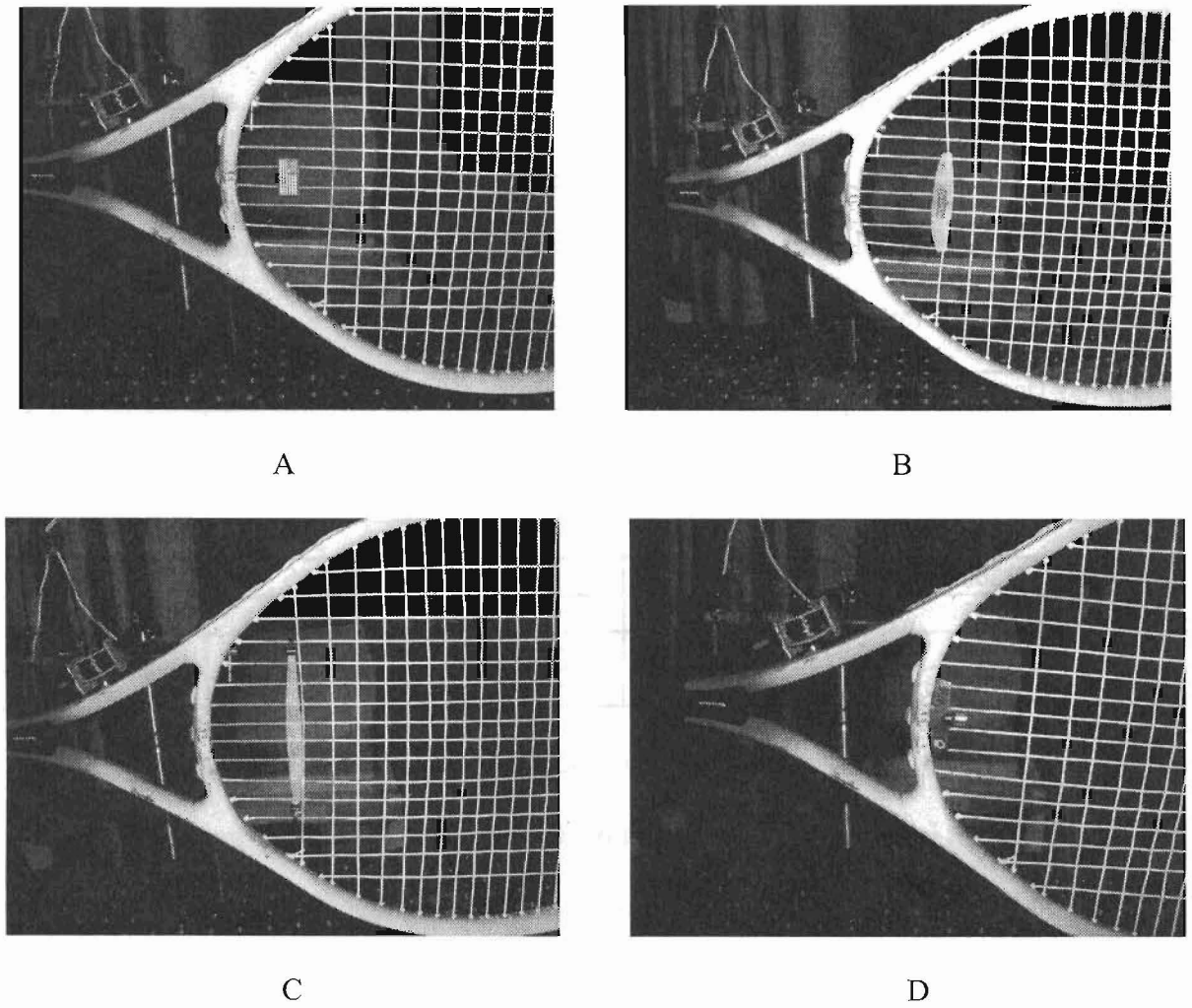

Figure 14: Vibration dampers attached to racket, A) Wilson Vibra-Fun B) Prince NXG Silencer, C) Head Smartsorb, D) Babolat RVS

All four models are made primarily of flexible rubber-like materials. The Prince and Wilson models are similar in that they attach to the racket by wedging between several strings. In this way, they are in contact with several strings, though the Prince model is in contact with several more than the Wilson model. The Head model winds between several strings in such a way that for each string, the vibration damper crosses the string on the opposite side compared to the lowest perpendicular string. It is also pressed up against this perpendicular string. The Babolat model is perhaps the most unique in that it is wedged between several strings, similar to the

Prince model, but it also rests against the frame and has attached to it a small metal weight. The masses of the four models are: Wilson) 2.32 g, Prince) 5.92 g, Head) 2.43 g, and Babolat 6.71 g.

4.3: Comparison of Mode Shapes and Mode Frequencies

The mode frequencies for the first eight modes of the tennis racket undamped and with the four models of vibration dampers can be seen in Table 3.

Mode	Freq. Undamped (Hz)	Freq. Wilson (Hz)	Freq. Prince (Hz)	Freq. Head (Hz)	Freq. Babolat (Hz)
1	47	47	47	47	47
2	113	113	112	112	111
3	125	125	124	125	123
4	323	322	320	321	321
5	569	588	611	515	not seen
6	895	918	not seen	991	908
7	916	not seen	not seen	not seen	916
8	1476	1434	not seen	not seen	1437

Table 3: The first eight modes of the undamped and damped racket.

From these results it is apparent that the vibration dampers have a relatively low effect on the first four modes of vibration of the tennis racket. However, they drastically alter the vibrational behavior of the tennis racket for the fifth through eighth modes. For instance, in the case of the Prince damper the sixth, seventh, and eighth modes are eliminated entirely. These modes will be discussed in order.

In addition to affecting the mode frequencies, the vibration dampers also heavily influenced the vibrational amplitude and in some cases the mode shapes of these higher modes. Interferograms of the first mode can be seen in Figure 15.

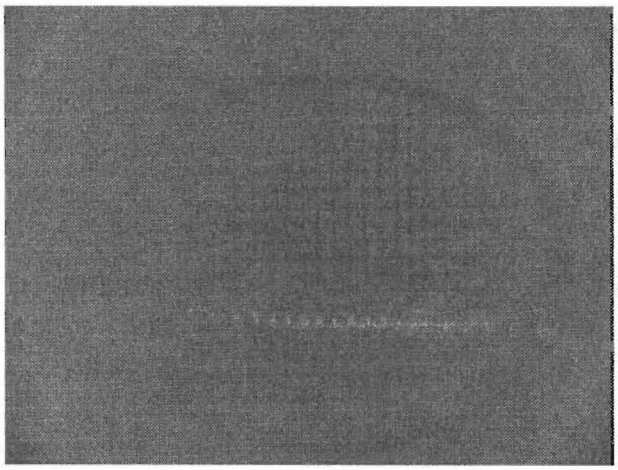

A

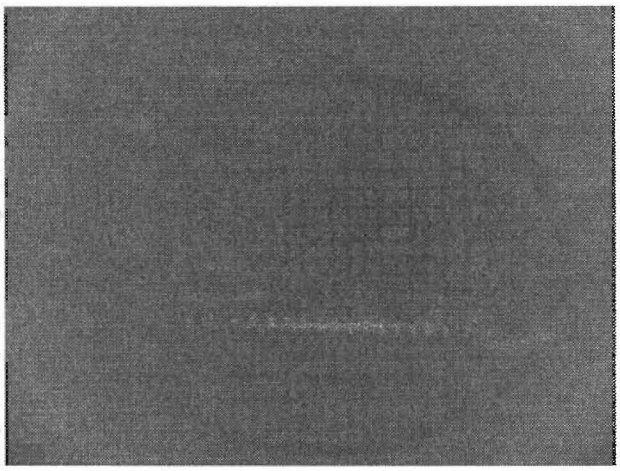

B

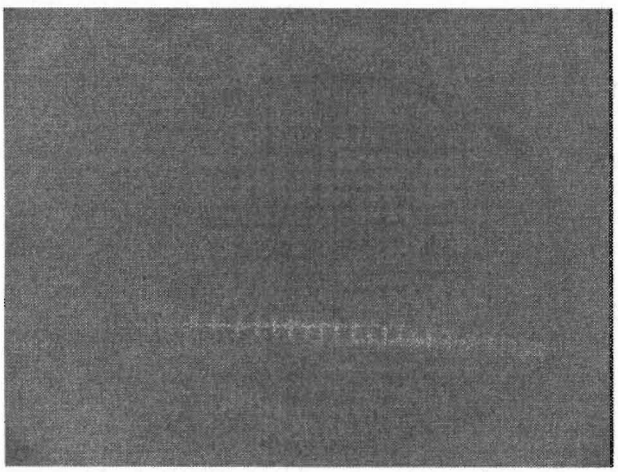

C

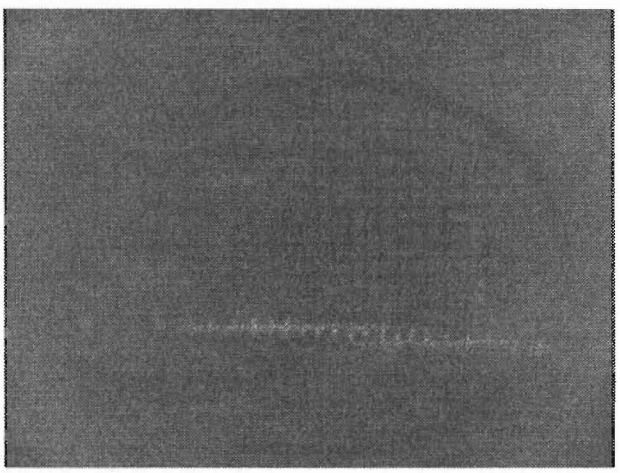

D

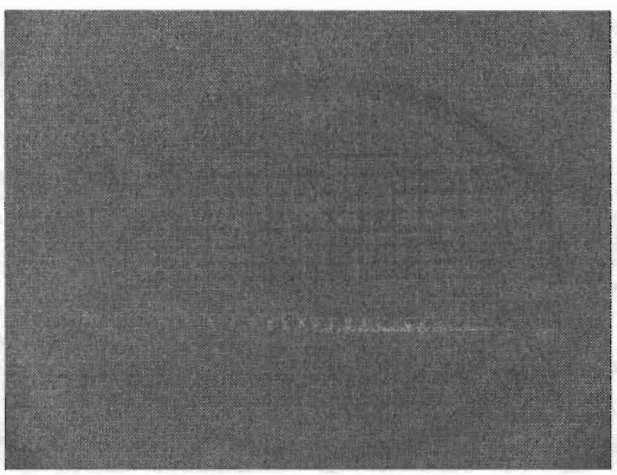

E

Figure 15: The first mode of a tennis racket: A) Undamped (47 Hz), B) Wilson (47 Hz), C) Prince (47 Hz), D) Head (47 Hz), E) Babolat (47 Hz)

In these interferograms a nodal line was seen that is roughly parallel to the main axis of the tennis racket. However, the nodal line was shifted significantly below the center line of the racket (the line from the tip of the handle to the tip of the head). This shift may be due to the method of vibration. The magnet was located on the top part of the throat, as can be seen in Figure 12. It is possible that since the vibration was applied in a asymmetric way, the mode shape is asymmetric. Similar behavior was seen in the third and fourth modes.

The primary observation to note about the first mode was that for all five cases the mode shapes and mode frequencies were remarkably similar. The Prince and Head vibration dampers may be damping the vibrations slightly, since the nodal line is wider, but this impact was not large.

Another important observation was that the strings and the racket frame were part of the nodes and anti-nodes. This seems to indicate that the racket was behaving as one body. Similar behavior was seen in the third and fourth modes.

The second mode of vibration of the tennis racket can be seen in Figure 16.

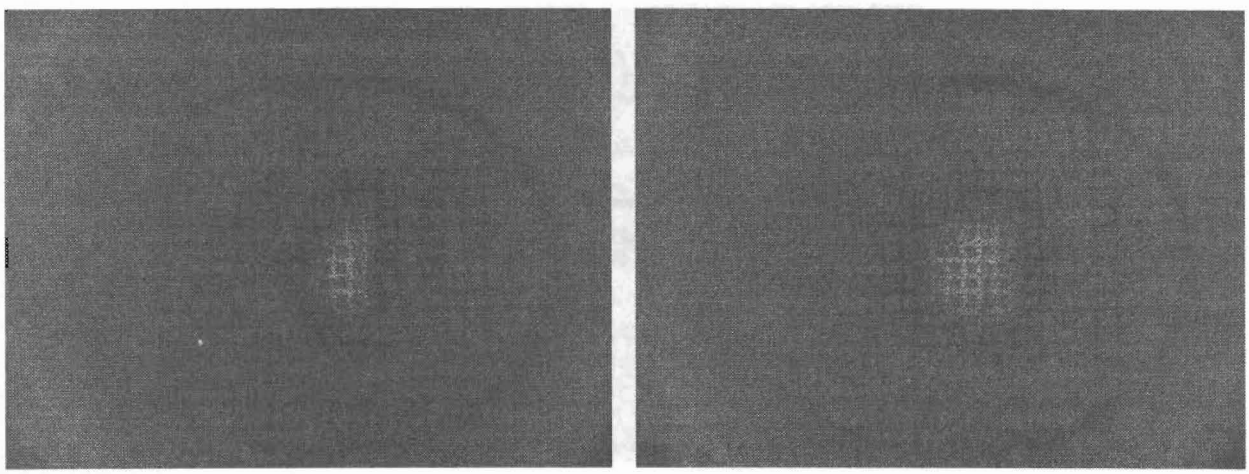

A B

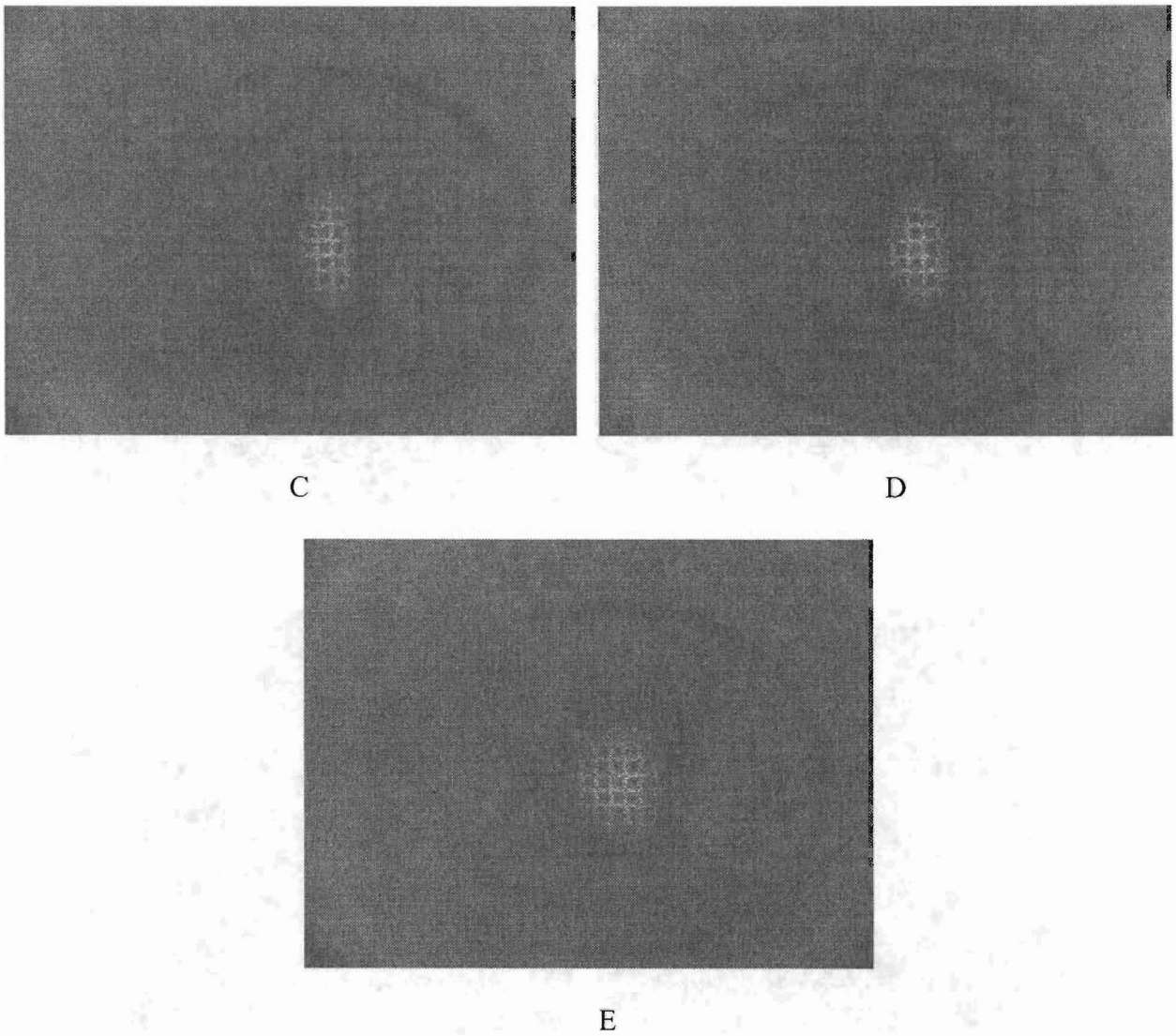

Figure 16: The second mode of a tennis racket: A) Undamped (113 Hz), B) Wilson (113 Hz), C) Prince (112 Hz), D) Head (112 Hz), E) Babolat (111 Hz)

The mode shapes observed for the second mode of the tennis racket were interesting due to the presence of what we describe as a nodal dot. Usually nodes are seen as lines from a boundary to another boundary, or in the form of a circle or ellipse. Here, though, a bright region characteristic of a node was clearly seen. Again, the vibration dampers did not significantly alter the mode frequency nor the mode shapes. The Prince, Head, and Babolat models did lower the mode frequency slightly. The Wilson and Babolat models seem to have enlarged the nodal dot, thus implying a decrease in vibrational amplitude, but this change was not large.

The third mode of vibration of the tennis racket can be seen in Figure 17.

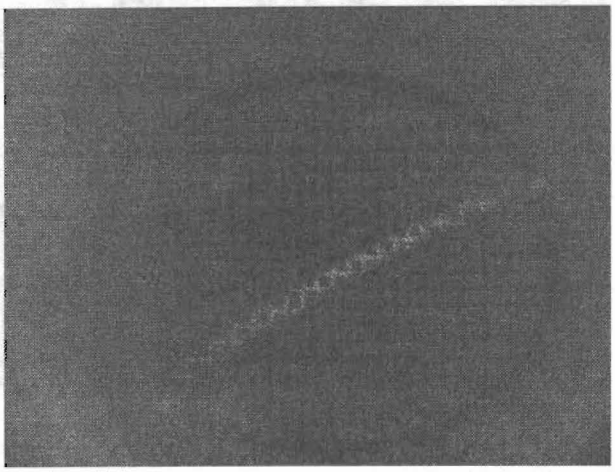

A

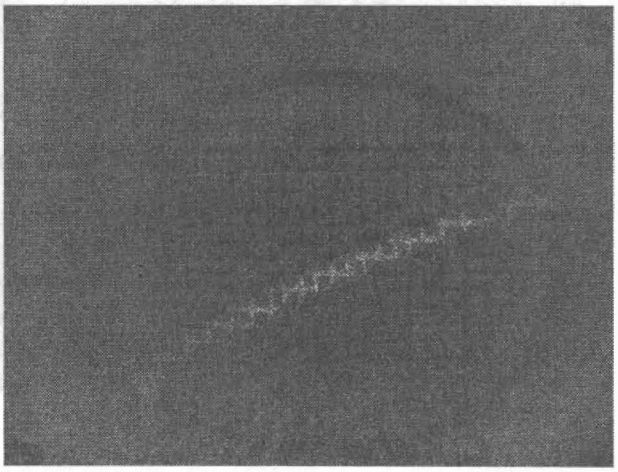

B

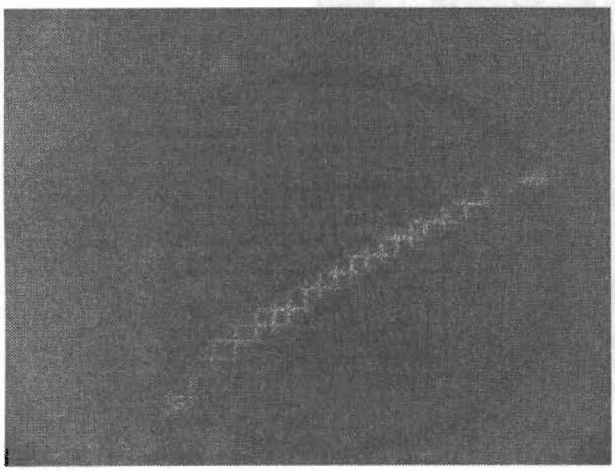

C

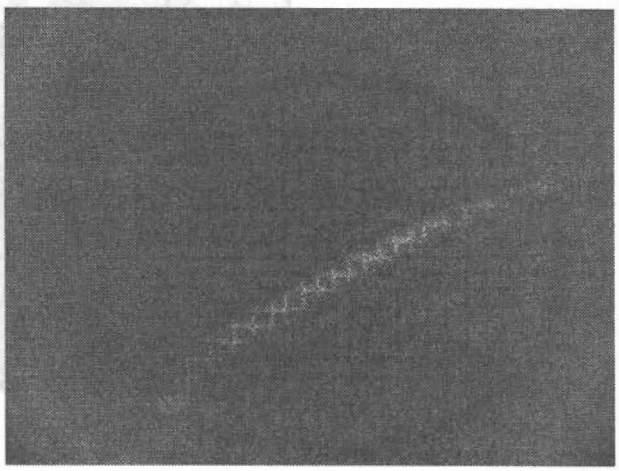

D

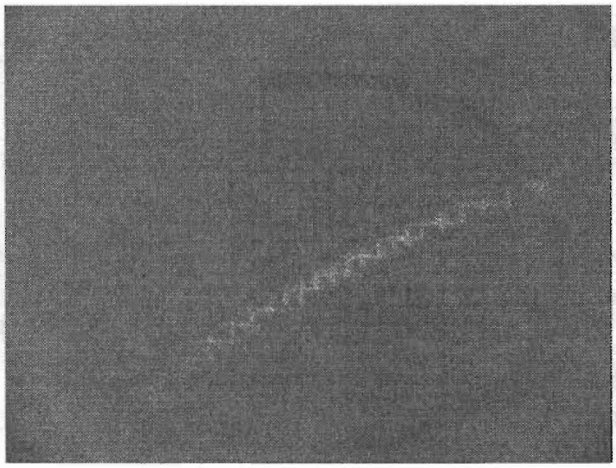

E

Figure 17: The third mode of a tennis racket: A) Undamped (125 Hz), B) Wilson (125 Hz), C) Prince (124 Hz), D) Head (125 Hz), E) Babolat (123 Hz)

The third mode shapes seen for the damped and undamped rackets are nearly identical with nearly identical frequencies. As was seen in the first mode, the node and anti-nodes were observed in both the strings and the frame. The asymmetric mode shape observed for the third mode may be due to the asymmetric method of vibration, as was discussed for the first mode. If the racket had been symmetrically vibrated, the node would form an arch from the edge of the racket near the ten o'clock position (if the racket head is thought of as a clock face) through the center of the racket and the two o'clock position [8, 33].

The fourth mode of vibration of the tennis racket can be seen in Figure 18.

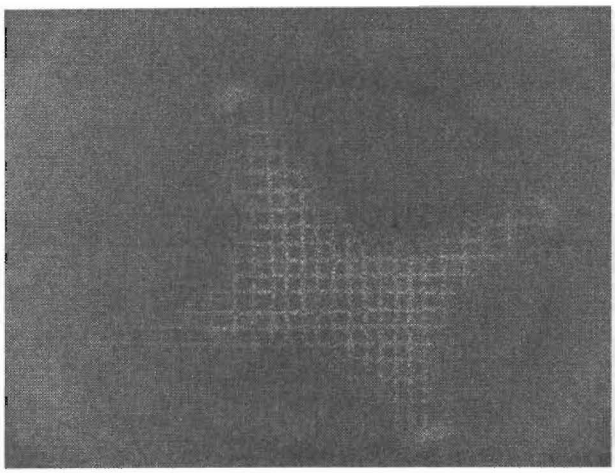

A

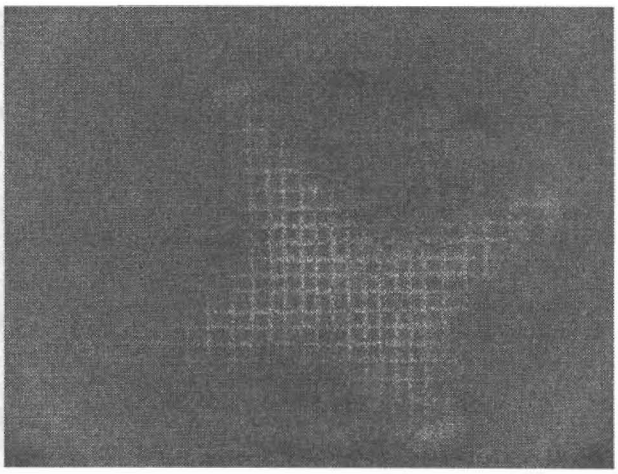

B

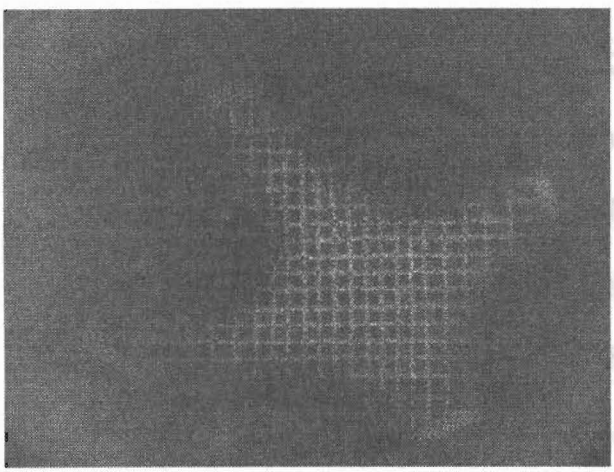

C

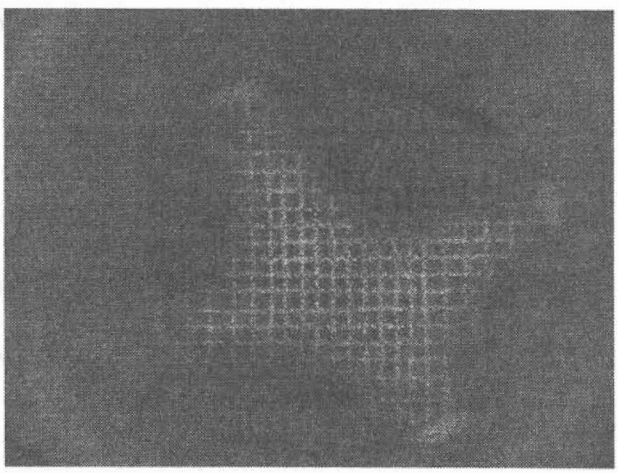

D

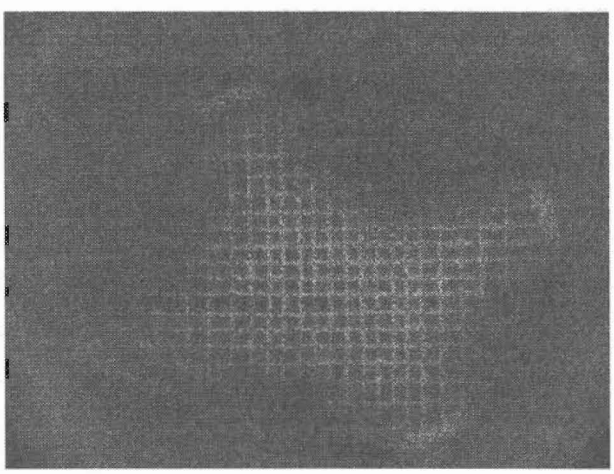

E

Figure 18: The fourth mode of a tennis racket: A) Undamped (323 Hz, 20 amp), B) Wilson (322 Hz, 19 amp), C) Prince (320 Hz, 18 amp), D) Head (321 Hz, 20 amp), E) Babolat (321 Hz, 18 amp)

Yet again, the vibration dampers only slightly altered the mode shape, mode frequency, and vibrational amplitude of the mode. The Babolat model may have slightly lowered the vibrational amplitude, but the driving vibrational amplitude for the Babolat model was lower than that applied to the undamped racket. The driving vibrational amplitude was lowered for the Babolat model because it was found that a higher driving amplitude "overdrove" the racket. In other words, at higher driving amplitudes the racket vibrations become unstable and no useful information could be gained.

As with the first and third modes, both the nodal region and the anti-nodes extended into the racket frame and the strings. The method of vibration may have caused the asymmetric nodal region seen in the fourth mode.

The fifth mode of vibration of the tennis racket can be seen in Figure 19.

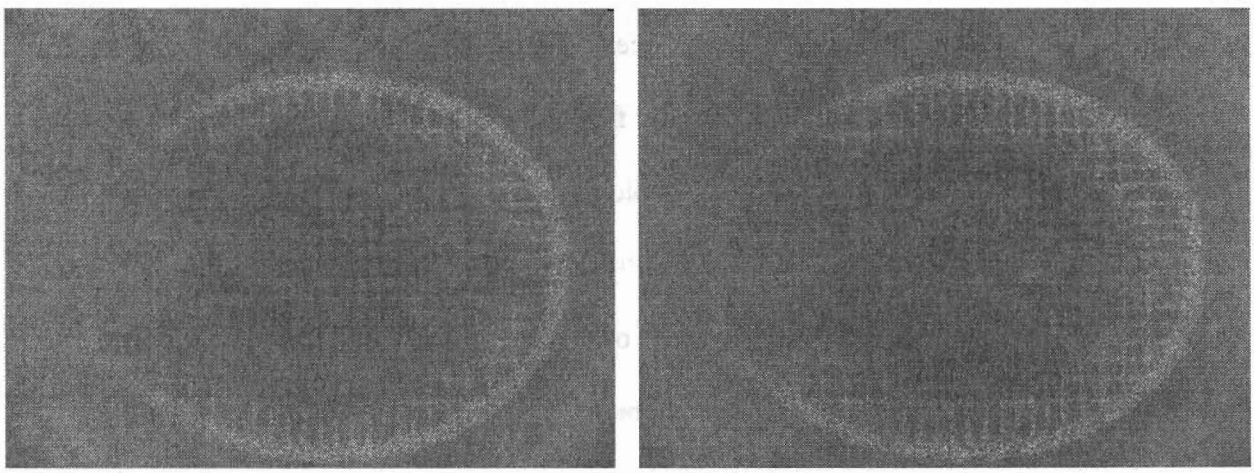

A B

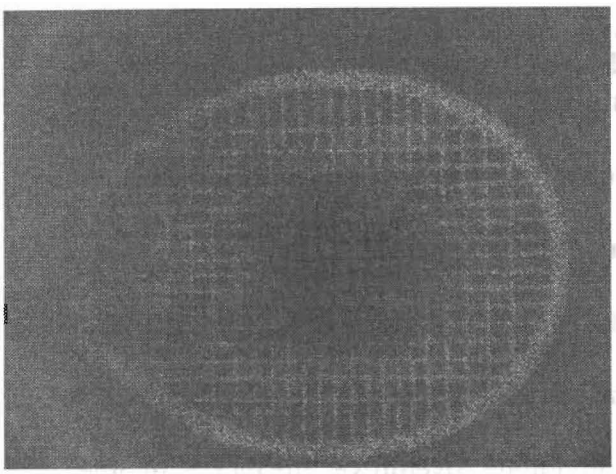

C

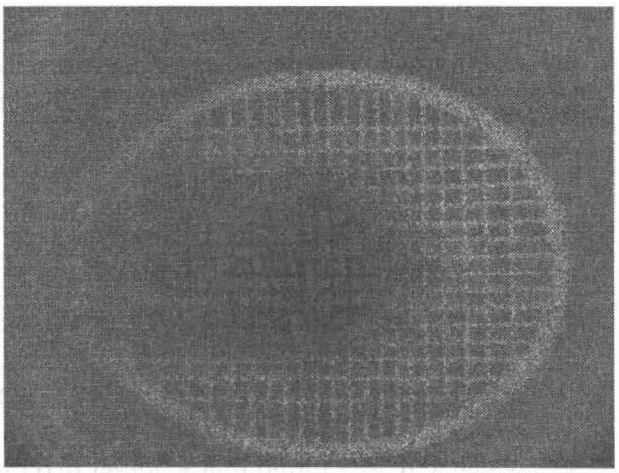

D

Figure 19: The fifth mode of a tennis racket: A) Undamped (569 Hz), B) Wilson (588 Hz), C) Prince (611 Hz), D) Head (515 Hz), Babolat not seen

From the interferograms in Figure 19, it clearly was seen that the vibration damping systems have had a large effect on the fifth mode. All four models lowered the vibrational amplitude of the fifth mode, though the Wilson model did not lower the vibrational amplitude as much as the other three models. The Prince and Head models lowered the vibrational amplitude significantly and the Babolat model eliminated the appearance of this mode entirely. Also, the Wilson and Prince models shifted the fifth mode to a higher frequency by 3.34% and 7.38% respectively. The Head model, while producing a similar mode shape as the Prince model, shifted the mode frequency lower by 9.49%. Finally, the node in this mode was present in the frame and the anti-node was wholly contained in the string section of the racket. Starting with the fifth mode, the racket head behaved as if the strings are a membrane or plate clamped at the edges and the racket frame always appeared as a node.

The sixth mode of vibration of the tennis racket can be seen in Figure 20.

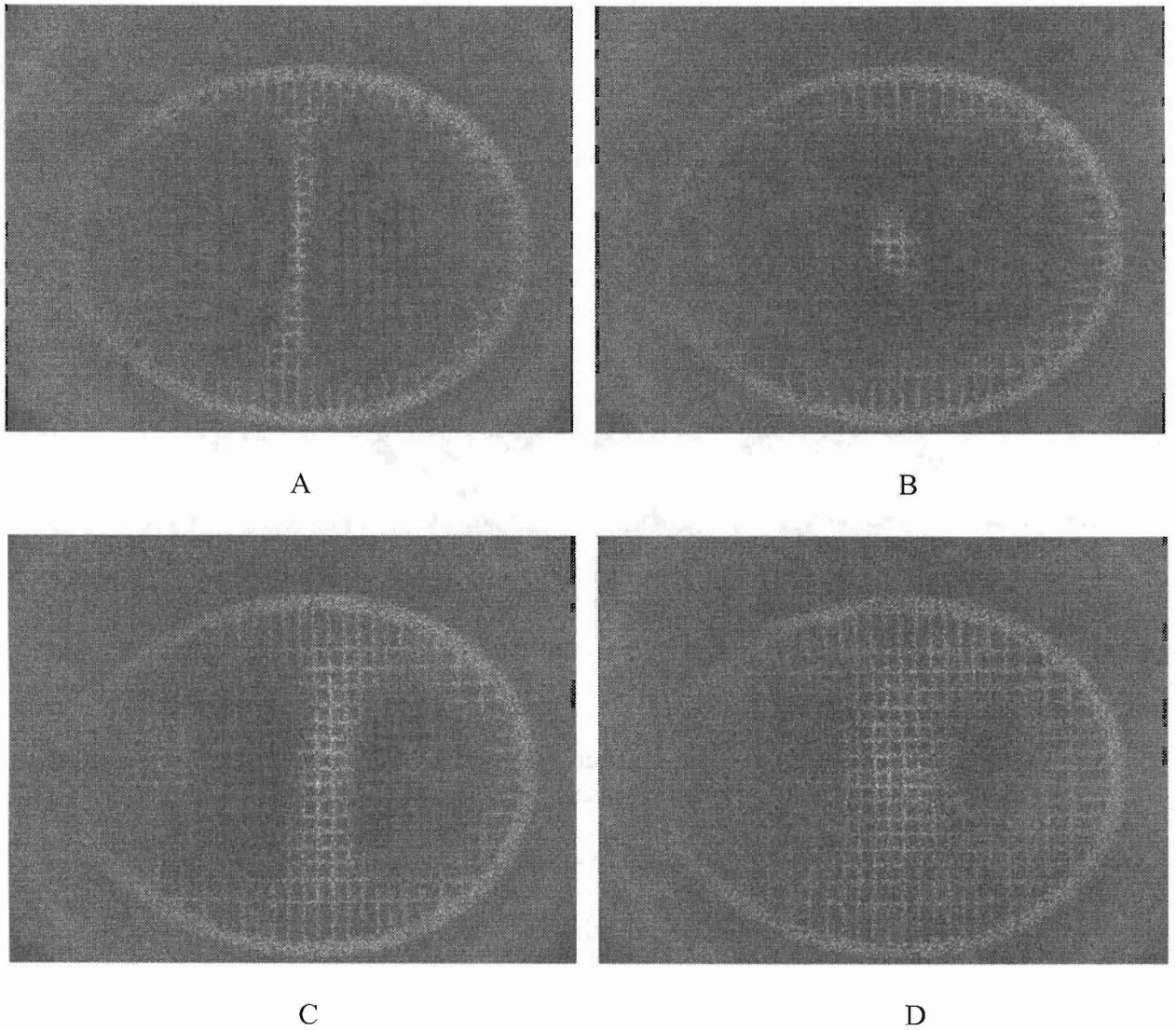

Figure 20: The sixth mode of a tennis racket: A) Undamped (895 Hz), B) Wilson (918 Hz), C) Head (991 Hz),D) Babolat (908 Hz), Prince not seen

Again, the vibration damping systems have clearly had a large effect on the sixth mode of the tennis racket. All models decreased vibrational amplitude, with the Wilson model having the least influence, the Head and Babolat models lowered the vibrational amplitude significantly, and the Prince model eliminated the appearance of the mode all together. The Head and Babolat models shifted the mode frequency higher by 10.7% and 1.45% respectively. The Wilson model altered the mode shape in that the nodal line through the center of the racket is reduced to nearly

a dot. In addition, the Wilson model shifted the mode frequency higher by 2.57%. Again, the anti-nodes were only present in the strings.

The seventh mode of vibration of the tennis racket can be seen in Figure 21.

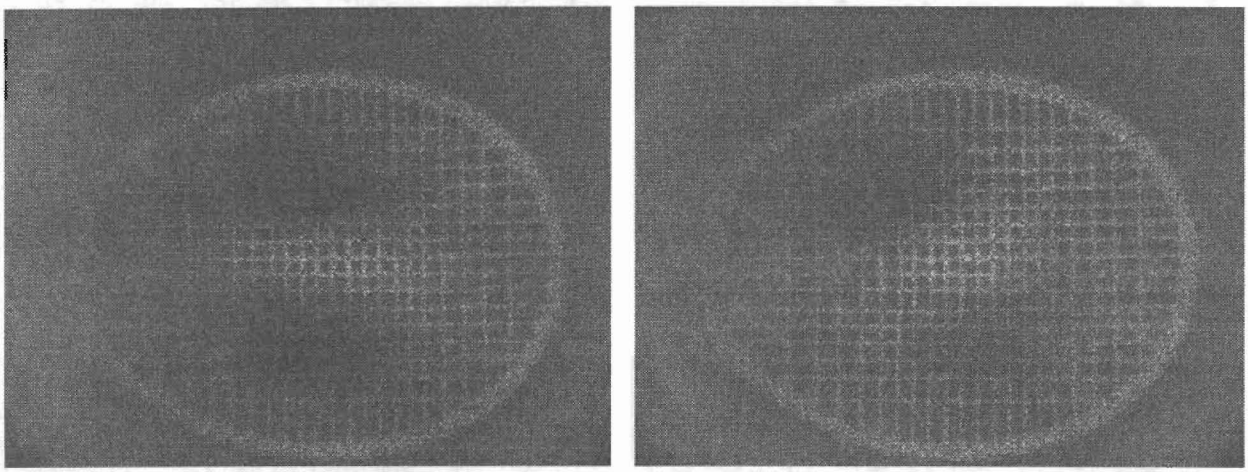

A B

Figure 21: The seventh mode of a tennis racket: A) Undamped (916 Hz, 23 amp), B) Babolat (916 Hz, 20 amp), Wilson not seen, Prince not seen, Head not seen

The vibrational damping systems influenced the seventh mode significantly. The Wilson, Prince, and Head models eliminated the appearance of the seventh mode entirely. As can be seen in the interferogram for the undamped racket, the seventh mode is not a particularly strong mode in comparison to the others studied. Therefore, the elimination of the appearance of this mode may not be remarkable. The Babolat model produced a mode shape that was rotated by approximately 45°. This may be due to the non-symmetric vibration method, though this non-symmetric behavior was not seen in the undamped racket. Interestingly, though all four models shifted the mode frequencies for the fifth and sixth modes, the mode frequency was not shifted by the Babolat model. Again, the anti-nodes were only present in the strings.

The eighth mode of vibration of the tennis racket can be seen in Figure 22.

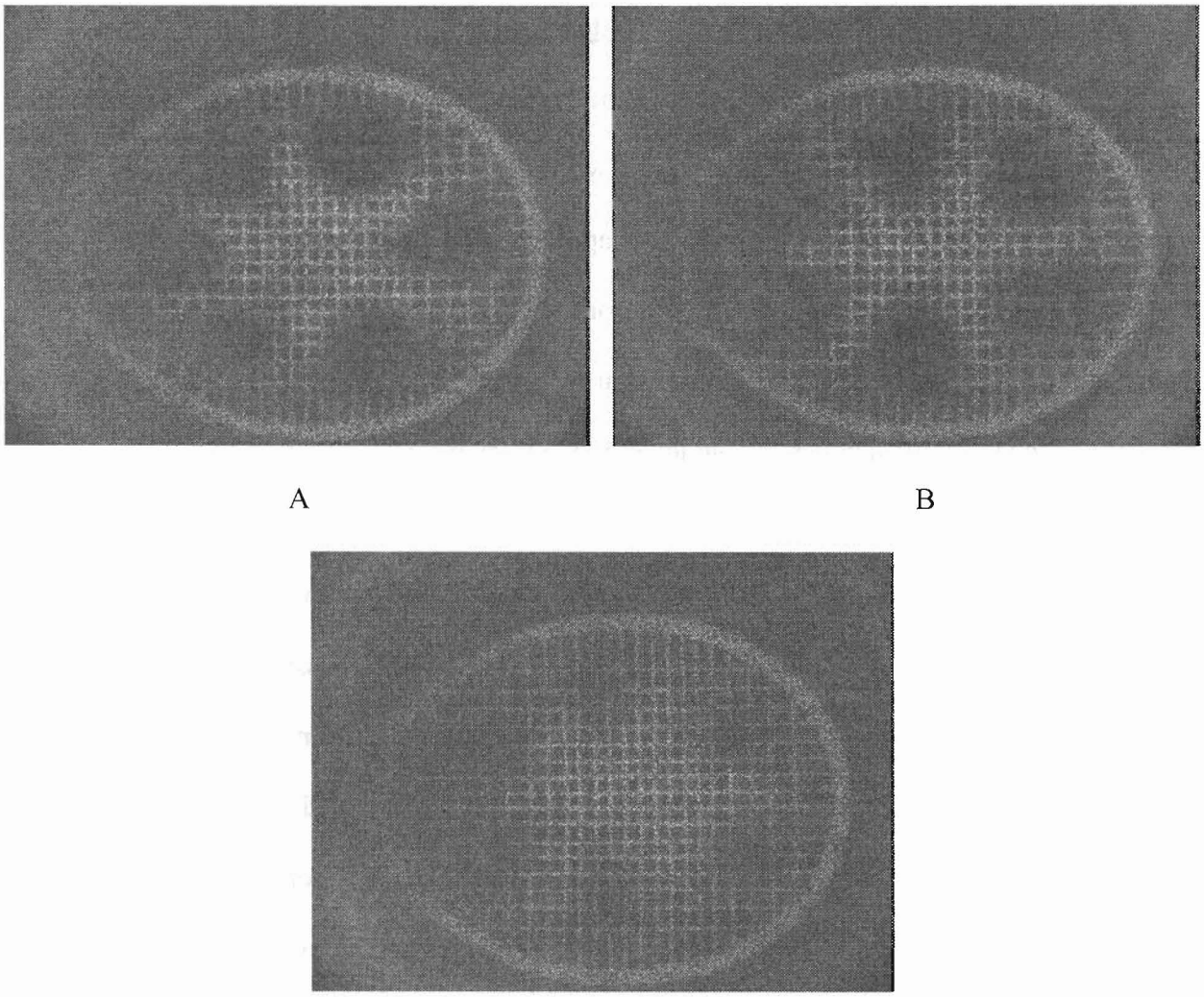

Figure 22: The eighth mode of a tennis racket: A) Undamped (1476 Hz), B) Wilson (1434 Hz), C) Babolat (1437 Hz), Prince not seen, Head not seen

The eighth and final mode examined also exhibited influence from the vibration dampers. The Prince and Head models eliminated the appearance of the mode entirely. The Wilson and Babolat models lowered the vibrational amplitude somewhat, but both rotated the mode shape. In the undamped racket, two regions of vibration were seen along the main axis of the racket. With the Wilson and Babolat models in place a nodal line was seen along the main axis. Also, the anti-nodes are only present in the strings, as was seen in the fifth, sixth, and seventh modes.

4.4: Discussion of Mode Frequencies and Mode Shapes

The vibration dampers studied significantly reduced the vibrational amplitude of the fifth through eighth modes of vibration of the racket while leaving the first four modes relatively intact. In addition, some models eliminated the appearance of modes entirely. Alteration of mode shape was seen for some vibration dampers at some frequencies: the Babolat model at the seventh mode, the Wilson and Babolat models at the eighth mode. It was expected that the presence of the vibration dampers would lower mode frequencies due to the addition mass of from the vibration damper. This behavior was seen for some models at some modes (see Table 3). However, some models raised the mode frequency: the Wilson and Prince models at the fifth mode, the Wilson, Head, and Babolat models at the sixth mode. One possible hypothesis for this behavior is that the presence of the vibration dampers increased string tension. We would expect that higher string tension, similar to a plate with a higher stiffness, would raise the mode frequencies. However, further experimentation should be conducted to conclude whether string tension is responsible for raised mode frequencies. Finally, the first four modes and the later four modes differ greatly in the presence of the anti-nodes exclusively in the strings for the later four modes. In this way, for the first four modes seem to represent the racket as behaving as one body, whereas the later four modes seem to represent the strings behaving similar to a membrane or plate clamped at it edges (in this case, the clamp is the racket frame).

While these findings are not in direct opposition with the findings of other research, they certainly draw interesting contrasts. For instance, Brody found that the vibration dampers did not affect the time it takes for vibrations to die out following an impact, nor do they affect the frequency of the racket vibrations [7, 8]. In this project, the time taken for cessation of vibration following an impact was not studied, so no comparison can be made. With regards to the

frequency of vibration, perhaps the higher modes that were damped in this project do not contribute largely to the overall vibrations seen in a racket following an impact. Stroede found that vibration dampers have no effect on the feel of the racket as experienced by the player [6]. Li found that vibration dampers do not reduce the vibrations felt by the hand and arm with regards to the approximately 120 Hz resonance of their racket [5]. This project did not measure the vibrations felt by the hand (or in this case the vibrations felt by the clamp), so again, perhaps the higher modes that were damped in this project do not contribute largely to the vibrations felt by the hand following an impact.

In the future, it would be worthwhile to construct a clamping system that better models the human hand and is able to detect vibration. Also, with the addition of a high speed camera to the SPI system, the vibrations of a tennis racket following an impact with a tennis ball could be observed and studied. Finally, in order to truly assess the cause of the asymmetric mode shapes, studies of the mode shapes should be conducted with several magnet locations.

4.5: Sweet Spot Controversy

There has been a fairly large amount of disagreement within the literature regarding the "sweet spot" of a tennis racket [8, 29, 31, 32, 34, 36]. Tennis players generally refer to the sweet spot as the region of the racket face where, if the ball is struck there, the hit "feels good" or "feels effortless" to the player and the ball travels large distances. This project did not hope to address the feel associated with ball-racket impacts on various parts of the racket, nor the relationship between the ability of the racket to impart a large velocity on the ball and the location of the impact. However, several authors consider the possibility that the sweet spot is a node of a particularly strong low frequency mode of vibration [8, 29, 31, 32, 34, 36]. By using speckle-pattern interferometry, this project has been able to clearly identify the nodal regions of

the low frequency modes. Furthermore, several authors have noted that the average impact time of a tennis ball (approximately 5 ms) is roughly one half of a cycle of vibration for modes near 100 Hz [32, 34]. Thus, when the ball is struck in the nodal region, less energy is spent in stretching the racket face and more energy is imparted to the ball than if the ball had struck an anti-node. There is some ambiguity regarding precisely which mode is responsible for this behavior. For instance, Brody clams the main mode responsible for this behavior is the arch shaped mode (the third mode as it is being referred to here) and that this is the fundamental mode [8]. Regardless of precisely which mode is responsible, from the mode shapes observed here it is apparent that the nodes of the first, second, third, fourth, and seventh modes all overlap in roughly the area of the nodal dot of the second mode. Thus, an impact in this area may be expected to not excite any of these modes, resulting in a larger amount of energy input to the ball.

5: Conclusion

Through the use of a Speckle-Pattern Interferometry system built and designed at Illinois Wesleyan University, a great deal of information has been gained about the vibrational behavior of a circular cured carbon fiber plate and a tennis racket. With regards to the carbon fiber plate, some effects of the orthogonal construction of the plate may have been detected in the mode shapes of the plate. Furthermore, the mode frequencies found for the plate do not correspond well with the theory available. Further research should be conducted to better understand the role of the method of vibration on the vibrational behavior of the disk. In addition, a better theoretical prediction of the mode frequencies should be sought.

The study of the tennis racket produced truly novel information in the form of never before seen interferograms of a tennis racket vibrating. Through the use of the SPI system, the

first eight modes of vibration were identified for a tennis racket clamped at the handle. Furthermore, the effects of vibration dampers on the vibrational behavior were found. The results indicate that all four models reduced high frequency mode vibration amplitude, though past research indicates that these reductions may not result in improved racket performance as advertised by the manufacturers.

6: Acknowledgements

I would like to thank the IWU students Tom Traynor, Alex Boecher, Sawyer Campbell and Kristy Streu for their efforts in constructing the SPI system and for their advice throughout research. Also, I would like to thank the IWU physical plant for expertly cutting the carbon fiber plate into a circle. In addition, I would like to thank Dr. Thomas Moore of Rollins College for his advice about the SPI system setup. Finally, and most of all, I would like to thank my advisor Dr. Andrew Morrison for his unending advice, support, and dedication.

7: References

1. T. D. Rossing, *Principles of Vibration and Sound* (Springer-Verlag, New York City, NY, 2004).
2. S. Chakraverty, "Free vibration analysis of elliptic and circular plates having rectangular orthotropy," Structural Engineering and Mechanics **7**, 53 (1999).
3. S. B. Dong, "Natural vibrations of a clamped circular plate with rectilinear orthotropy by least squares-collocation," Int. J. of Solids and Struct. **21**, 515 (1985).
4. C. S. Kim, "Natural frequencies of orthotropic, elliptical and circular plates," J. Sound and Vib. **259**, 733 (2003).
5. F. X. Li, "String vibration dampers do not reduce racket frame vibration transfer to the forearm," J. of Sports Sci. **22**, 1041 (2004).

6. C. L. Stroede, "The effect of tennis racket string vibration dampers on racket handle vibrations and discomfort following impacts," J. of Sports Sci. **17**, 379 (1999).

7. H. Brody, "Vibration damping of tennis rackets," Int. J. of Sports Biomechanics **5**, 451 (1989).

8. H. Brody, R. Cross, and C. Lindsey, *The Physics and Technology of Tennis* (Racquet Tech Publishing, Solana Beach, CA, 2002).

9. T. R. Moore, "A simple design for an electronic speckle pattern interferometer," AJP **72**, 1380 (2004).

10. T. R. Moore, "Interferometric studies of a piano soundboard," J. Accoust. Soc. Am. **119**, 1783 (2006).

11. O. J. Lokberg, "Interferometric comparison of displacements by electronic speckle pattern interferometry," App. Opt. **20**, 2630 (1981).

12. O. J. Lokberg, "Use of chopped laser light in electronic speckle pattern interferometry," App. Opt. **18**, 2377 (1979).

13. G. O. Rosvold, "Effect and use of exposure control in vibration analysis using TV holography," App. Opt. **32**, 684 (1993).

14. Wikipedia, http://en.wikipedia.org/wiki/Image:Laser_speckle.jpg, last modified 9-24-2005.

15. A forthcoming paper by T. R. Moore.

16. O. P. Bahl et. al., "Manufacture of Carbon Fiber," in *Carbon Fibers* edited by J. B. Donnet et. al. (Marcel Dekker, New York City, NY, 1998).

17. D. D. L. Chung, *Carbon Fiber Composites* (Butterworth-Heinemann, Newton, MA, 1994).

18. T. D. Rossing, "Chladni's law for vibrating plates," Am. J. Phys. **50**, 271 (1982).

19. E. F. F. Chladni, *Die Akustik* (Breitkopf und Härtel, Leipzig, 1802 and 1803).

20. M. D. Waller, *Chladni Figures: A Study in Symmetry* (Bell, London, 1961).

21. A. W. Leissa, "Recent research in plate vibrations: Classical Theory," Shock and Vib. Digest **9**, 13 (1977).

22. A. W. Leissa, "Plate vibration research, 1976-1980: classical theory," Shock and Vib. Digest **13**, 11 (1981).

23. A. W. Leissa, "Plate vibration research, 1976-1980: complicating effects," Shock and Vib. Digest **13**, 17 (1981).

24. A. W. Leissa, "Recent studies in plate vibrations, 1981-1985: part 1. classical theory," Shock and Vib. Digest **19**, 11 (1987).

25. A. W. Leissa, "Recent studies in plate vibrations, 1981-1985: part 2. complicating effects," Shock and Vib. Digest **19**, 10 (1987).

26. A. P. French, *Vibrations and Waves* (W. W. Norton and Company Inc., New York City, NY, 1971).

27. J. Kotze, "The role of the racket in high speed tennis serves," Sports Eng. **3**, 67 (2000).

28. R. Cross, "Center of percussion of hand-held implements," Am. J. Phys. **72**, 622 (2004).

29. R. Cross, "The sweet spots of a tennis racket," Sports Eng. **1**, 63 (1998).

30. H. Brody, "The physics of tennis: III the ball-racket interaction," Am. J. Phys. **65**, 981 (1997).

31. H. Brody, "The physics of the tennis racket: II the "sweet spot"," Am. J. Phys. **49**, 816 (1981).

32. S. J. Haake, "The dynamic impact characteristics of tennis balls with tennis rackets," J. of Sports Sci. **21**, 839 (2003).

33. J. E. Oh, "A study on the dynamic characteristics of tennis racket by modal analysis," Bull. of JSME **29**, 2228 (1986).

34. M. Brannigan, "Mathematical modeling and simulation of a tennis racket," Med. and Sci. in Sports and Exercise **13**, 44 (1981).

35. H. Brody, "Models of tennis racket impacts," Int. J. of Sport Biomechanics **3**, 293 (1987).

36. R. Cross, "The dead spot of a tennis racket," Am. J. of Phys. **65**, 754 (1997).